Sea surface temperatures of southern midlatitudes 0–160 kyr B.P.

Katharina Pahnke[1,2] and Julian P. Sachs[1,3]

Received 4 July 2005; revised 7 November 2005; accepted 11 January 2006; published 13 April 2006.

[1] Late Quaternary climate fluctuated between extremes of glaciations, lasting ~90 kyr on average, and interglacial episodes, lasting ~10 kyr. Still largely unknown are the spatial and temporal evolution of these global climate states, with vigorous debate still underway on the mechanisms responsible for glacial inceptions and terminations. Though it is widely believed that the Southern Hemisphere oceans play a central role in global climate changes, few paleoclimate records exist from there. Here we present three new alkenone-derived SST records from the midlatitude Southern Hemisphere spanning the last 160 kyr, a full glacial-interglacial cycle. Our subtropical SST records from the last glacial period are characterized by (1) warming 47–23 kyr B.P., when high latitudes in both hemispheres cooled, and (2) milder temperatures during the penultimate glacial period than during the last glacial interval. These SST features are found to be of tropical- to subtropical-wide extent, implying increased thermal gradients at times of high-latitude ice sheet growth. This has implications for the vigor of atmospheric and upper ocean circulation and the transport of heat and moisture to the poles that may have been instrumental in the growth and maintenance of polar ice sheets during glacial periods.

Citation: Pahnke, K., and J. P. Sachs (2006), Sea surface temperatures of southern midlatitudes 0–160 kyr B.P., *Paleoceanography*, *21*, PA2003, doi:10.1029/2005PA001191.

1. Introduction

[2] Polar ice core climate records, the $\delta^{18}O$ composition of the calcareous tests of benthic and planktonic foraminifera and SST records provide the main basis for our present understanding of climatic changes of the recent geologic past. The development of two new paleotemperature proxies, the Mg/Ca ratio in planktonic foraminifera [e.g., *Nürnberg*, 1995; *Nürnberg et al.*, 1996; *Elderfield and Ganssen*, 2000] and the unsaturation ratio of alkenones ($U^{K'}_{37}$-index) [*Brassell et al.*, 1986; *Prahl et al.*, 1988; *Müller et al.*, 1998] has led to the recent increase in direct SST reconstructions. However, despite a significant number of SST reconstructions from Southern Hemisphere latitudes, the main focus has so far been on the mid- to high-latitude North Atlantic. Partly as a consequence of this, the perception of the origin of climatic changes is biased toward the North Atlantic as the main agent in triggering climatic reorganizations. Yet, the mid-southern latitudes play an important role in the communication and signal transfer between low and high latitudes and between the Southern and Northern Hemispheres. Moreover, they constitute the main moisture source for Antarctic precipitation [*Delaygue et al.*, 2000]. SST changes in the midlatitudes therefore exert a potentially critical influence on the moisture supply to high latitudes and hence the growth and decay of polar ice sheets in the course of glacial-interglacial and shorter-term climatic changes.

[3] Paleo-SST records from the mid and high latitudes of the Southern Hemisphere are still sparse owing to the difficulty in obtaining continuous marine sediment profiles from this region with its carbonate-corrosive water masses and rough seas. However, available records have confirmed the global extent of glacial-interglacial climate variations and the lead of temperature over ice volume changes observed in the tropics and high southern latitudes [e.g., *Howard and Prell*, 1992; *Schneider et al.*, 1995; *Weaver et al.*, 1998; *Mashiotta et al.*, 1999; *Schneider et al.*, 1999; *Lea et al.*, 2000; *Calvo et al.*, 2001a; *Sachs et al.*, 2001; *Sikes et al.*, 2002]. Detailed examination of the SST records from low to mid latitudes, however, has revealed differences to the high-latitude temperature evolution in several instances. For example, *Schneider et al.* [1999] presented several paleo-SST records from the tropical and subtropical South Atlantic and found, deviating from high-latitude temperatures, warmer SSTs during MIS6a than during the Last Glacial Maximum (LGM) and a temperature minimum prior to the LGM. The authors attributed these differences to a low-latitude temperature response to precession-driven insolation forcing and the transfer of this signal to midlatitudes. In contrast, a differential temperature evolution in the subtropical and high-latitude North Atlantic at the end of MIS5e has been suggested to reflect the dominant influence of mean annual insolation that is solely driven by obliquity changes and hence exhibits opposite trends north and south of ~43°N [*Cortijo et al.*, 1999]. Similarly, *Sachs et al.* [2001] suggested a prominent obliquity signal in a sea surface temperature record from the southeast Atlantic between ~40 and 20 kyr B.P. The authors proposed a link between the observed temperature pattern and the deuterium excess record from Antarctic ice cores that shows a dominant obliquity cycle and has previously been interpreted in terms of SST variability at the moisture source (the mid-southern latitude oceans) or shifts in the source area in

[1]Department of Earth, Atmospheric and Planetary Sciences, Massachusetts Institute of Technology, Cambridge, Massachusetts, USA.
[2]Now at Lamont-Doherty Earth Observatory of Columbia University, Palisades, New York, USA.
[3]Now at School of Oceanography, University of Washington, Seattle, Washington, USA.

0883-8305/06/2005PA001191

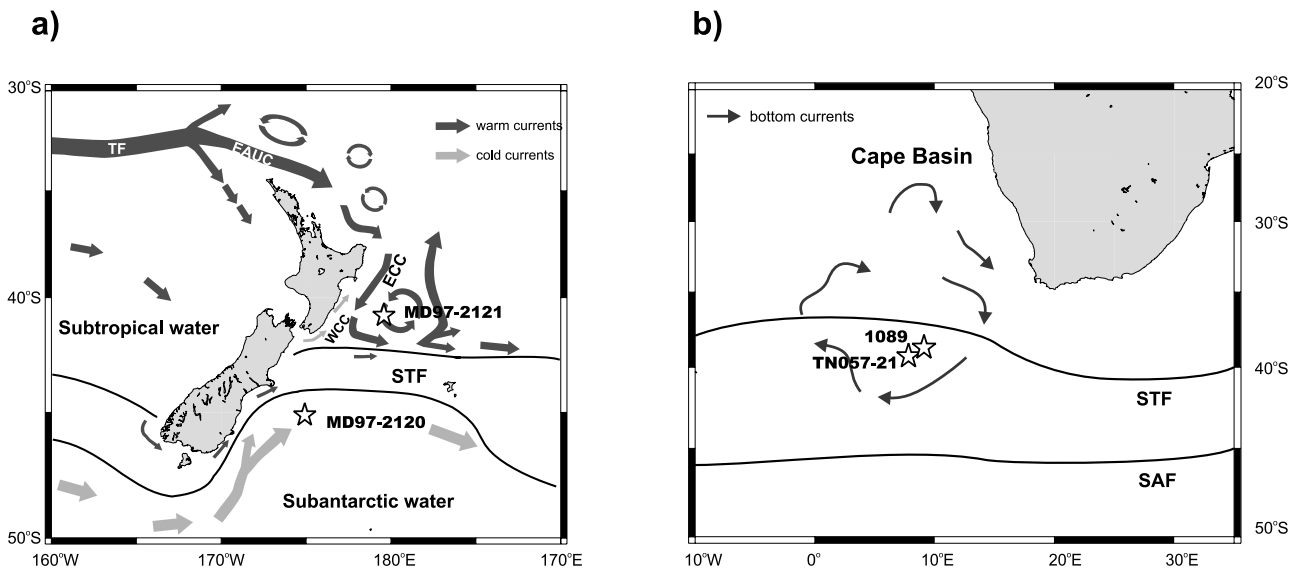

Figure 1. Core locations and local oceanography. (a) Location of cores MD97-2121 and MD97-2120 to the north and south of Chatham Rise, east of New Zealand, respectively. The Subtropical Front (STF, northern and southern front) [after *Carter et al.*, 1998; *Sutton*, 2001], that is part of the circum-Antarctic frontal system, separates warm, relatively saline subtropical waters from cold, fresh subantarctic waters. General circulation of warm and cold surface currents around New Zealand is shown schematically by dark- and light-gray arrows, respectively (re-drawn after *Carter et al.* [1998]). (b) Location of core TN057-21 and ODP Site 1089 in the Cape Basin, southeast Atlantic. Gray arrows indicate flow of bottom currents that result in erosion in the northern Cape Basin and sediment deposition on the sediment drifts at the southern boundary of the basin [after *Tucholke and Embley*, 1984]. Alkenone sea surface temperature estimates have therefore been suggested to reflect subtropical (northern Cape Basin) conditions [*Sachs and Anderson*, 2003]. SAF, Subantarctic Front.

response to obliquity-driven changes in the thermal gradient between mid and high latitudes [*Vimeux et al.*, 1999, 2001, 2002]. Source temperature reconstructions for Greenland ice (GRIP ice core) and the calculated temperature gradient between Greenland and its moisture source (suggested to be the tropical to subtropical oceans) also reveal a strong parallelism with obliquity during the last glacial period [*Masson-Delmotte et al.*, 2005]. An alkenone-derived SST record from the subtropical southeast Pacific, on the other hand, exhibits a dominant eccentricity cycle over most of the past 400 kyr, with SST changes following high-latitude obliquity variations at times of low eccentricity [*Calvo et al.*, 2001a]. These studies demonstrate the potential of low- to mid-latitude climates to change independently from those at high latitudes. To further examine the climate response of the midlatitudes and their role in the global climate system, we have generated and extended alkenone sea surface temperature records from the midlatitudes of the southeast Atlantic and southwest Pacific that span the past 160 kyr. We find that the subtropical SST evolution is consistent with that seen in other paleo-SST records from the tropical to subtropical latitude belt of both hemispheres but distinct from that at high latitudes.

2. Materials and Methods

2.1. Core Locations and Oceanographic Settings

[4] IMAGES cores MD97-2121 (40°22.8′S, 177°59.4′E, 3014m water depth) and MD97-2120 (45°32.06′S, 174°55.85′E, 1210m water depth) are located east of New Zealand to the north and south of the west-east trending submarine Chatham Rise, respectively (Figure 1 and Table 1). We extended the SST record of core MD97-2120 [*Sachs and Anderson*, 2005] to 19.3 m (156 kyr) and measured alkenone unsaturation ratios for SST estimation along the entire 35-m-long core MD97-2121.

[5] New Zealand's high mountain ranges and active volcanism lead to high terrigenous sediment influx into the ocean and hence sedimentation rates at the core sites of $\geq$30 cm/kyr (MD97-2121) [*Carter et al.*, 2002] and 10-20 cm/kyr (MD97-2120) [*Pahnke et al.*, 2003], with highest rates reached during past glacial periods when New Zealand's climate was dry and vegetation cover sparse [*Shane and Sandiford*, 2003]. Despite the high sediment load reaching the continental shelf and the high seismicity of New Zealand, neither of the core sites was affected by turbidity currents or mass failure in the past as indicated by the lack of turbidity current channels or scars [*Lewis et al.*, 1999], the intact hemipelagic sequences along the cores and no identifiable signs of sediment disturbances [*Carter et al.*, 2002; *Pahnke et al.*, 2003].

[6] The surface oceanography east of New Zealand is controlled by the Subtropical Front (STF), a hydrographic feature that is part of the circum-Antarctic frontal system and separates subtropical from subantarctic waters (Figure 1a). The STF in the study area is deflected south and wrapped around the southern tip of New Zealand from where it continues northeast along the east coast of South

Table 1. Location of Sediment Cores Presented in This Study

Core	Latitude	Longitude	Water Depth, m	Region
MD97-2121	40°22.8′S	177°59.4′E	3014	SW Pacific
MD97-2120	45°32.06′S	174°55.85′E	1210	SW Pacific
TN057-21-PC2	41°08′S	7°49′E	4981	SE Atlantic
ODP 1089	40°56.18′S	9°53.64′E	4621	SE Atlantic

Island as the Southland Current. Upon reaching Chatham Rise, the front bends to the east and follows the east-west orientation of the rise at about 44°S [*Sutton*, 2001]. The Southland Current splits with one branch following the STF while a small part continues its northeastward flow through Mernoo Saddle, a topographic depression at the western extent of Chatham Rise [*Chiswell*, 1996; *Carter et al.*, 1998; *Nelson et al.*, 2000].

[7] The surface circulation north of Chatham Rise is dominated by the East Cape Current (ECC) that flows southwest along the east coast of North Island as the extension of the East Auckland Current/Tasman Front. The ECC transports warm, high-salinity waters to Chatham Rise, where it is deflected eastward to continue along the STF [*Heath*, 1985]. East of the ECC lies the permanent Wairarapa Eddy, an anticyclonic surface feature that is centered at 41°00′S, 178°40′E [*Roemmich and Sutton*, 1998]. At present, there is no lateral particle transport in the upper 1000 m on either side of the Chatham Rise [*King and Howard*, 2001; *Sikes et al.*, 2005], suggesting that the sediment record is not affected by surface circulation and particle advection from other areas to the core sites.

[8] The STF marks the rapid transition from subantarctic waters in the south to subtropical waters in the north. The site of core MD97-2120 south of the STF is therefore influenced by the cold, low-salinity waters of the Subantarctic Zone (summer SST: 15.1°C, salinity 34.4 [*Uddstrom and Oien*, 1999; *Chiswell*, 2002]), while core MD97-2121 lies in warmer, more saline subtropical waters (summer SST: 18°C, salinity 35 [*Uddstrom and Oien*, 1999]).

[9] Core TN057-21-PC2 (41°08′S, 7°49′E; 4981 m water depth) was retrieved from a drift site in the southeast Atlantic just north of the Agulhas Ridge that marks the southern boundary of the Cape Basin. In order to obtain a continuous 0- to 160-kyr-long record we extended the previously published 110-kyr-long SST record of core TN057-21-PC2 [*Sachs and Anderson*, 2003] using samples from ODP Site 1089 (40°56.18′S, 9°53.64′E, 4621 m water depth) that is located on the same drift 176 km northeast of TN057-21-PC2 (combined record referred to in the following as TN057-21/1089). The temperature records show very similar SST values in the overlapping interval (Figure 3 in section 2.2.2).

[10] Vigorous cyclonic bottom currents in the Cape Basin result in erosion in the northern and northeastern part of the basin and sediment deposition at the core sites in the southern Cape Basin [*Tucholke and Embley*, 1984]. Consequently, although the core site is located in subantarctic waters, the paleo-records along the core document climatic conditions in the subtropical part of the Cape Basin [*Sachs and Anderson*, 2003]. This was inferred from core-top alkenone-derived SST estimates of core TN057-21-PC2 that are some 6°C warmer than the overlying surface waters at the core site [*Sachs et al.*, 2001]. Downcore SST variability shows no correlation with sediment focusing factors derived from unsupported ^{230}Th along the core, and closely covaries with SST changes at nearby nondrift sites [*Sachs and Anderson*, 2003]. This has been suggested to indicate that the SST variations along cores TN057-21-PC2/1089 consistently document subtropical surface conditions and are not an artifact of changes in sediment advection [*Sachs and Anderson*, 2003]. We will therefore interpret the SST record in terms of temperature changes in the subtropical part of the Cape Basin.

2.2. Methods

2.2.1. Alkenone Analysis

[11] Sample preparation and alkenone analysis followed standard protocols described by *Sachs and Lehman* [1999]. Briefly, freeze-dried sediment samples (4–5 g) were weighed into stainless-steel cells with an equivalent amount of sodium sulfate (dispersing and drying agent). Two micrograms of a recovery standard (Ethyl triacontanoate in 20% acetone in hexane) were added and the samples were extracted with dichloromethane at 150°C and 2000 psi on a Dionex ASE-200 pressurized fluid extractor. The total lipid extracts were dried under a N_2 stream, transferred into 2-mL autosampler vials and re-dissolved in 400 μL toluene containing 2 μg of *n*-hexatriacontane (*n*-C_{36}, a quantitation standard). Samples were derivatized with bis(trimethylsilyl)trifluoroacetamide for 1 hour at 60°C and alkenones (C_{37} methyl ketones) were quantified by capillary gas chromatography on an Agilent 6890N with a Chrompack CP-Sil-5 column (60 m by 0.32 mm inner diameter, 0.25-μm film thickness), a programmable temperature vaporization inlet in solvent-vent mode, and flame-ionization detector. The oven was programmed from 110°C to 270°C at 40°C/min followed by a temperature increase of 2°C/min to 320°C, and an 18-min isothermal period.

2.2.2. Alkenone Paleothermometry

[12] Long-chain alkenones, synthesized by haptophyte algae (notably *Emiliania huxleyi* and *Gephyrocapsa oceanica*) [*Volkman et al.*, 1980; *Marlowe et al.*, 1984; *Volkman et al.*, 1995], have become a useful tool in paleoceanography for the reconstruction of past sea surface temperatures and productivity. This application is based on the linear relation between the ratio of di- and tri-unsaturated C_{37}-alkenones ($U^{K'}_{37} = C_{37:2}/(C_{37:2} + C_{37:3})$) and ambient water temperature [*Brassell et al.*, 1986; *Prahl and Wakeham*, 1987; *Prahl et al.*, 1988]. The most widely used empirical equation for SST estimation from the $U^{K'}_{37}$-index was proposed by *Prahl et al.* [1988] on the basis of cultured *E. huxleyi* ($U^{K'}_{37} = 0.034T + 0.039$, $r^2 = 0.994$). A global compilation of alkenone analyses of surface sediments has confirmed this relation [*Müller et al.*, 1998] ($U^{K'}_{37} = 0.033T + 0.044$, $r^2 = 0.958$) and suggests that the $U^{K'}_{37}$ index is best correlated with mean annual SST overlying the core sites. For the Antarctic and sub-Antarctic, however, *Sikes and Volkman* [1993] demonstrated highest correlation of $U^{K'}_{37}$ in suspended particles with summer SSTs ($U^{K'}_{37} = 0.0414T - 0.156$, $r^2 = 0.958$), consistent with highest alkenone fluxes in this region

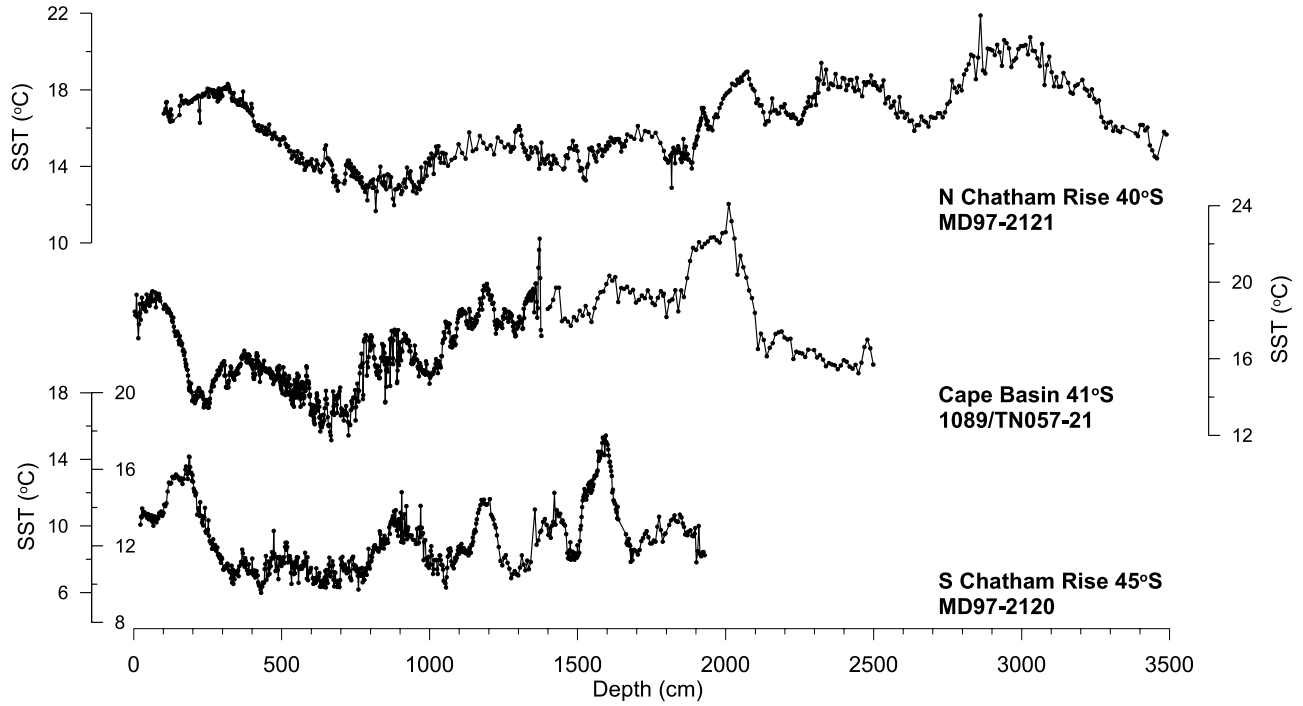

Figure 2. Alkenone SST records of cores MD97-2121 (north of Chatham Rise), TN057-21/1089 (Cape Basin), and MD97-2120 (south of Chatham Rise) versus depth in core. Outer SST axis for MD97-2120 using *Prahl et al.* [1988] calibration, inner axis using *Sikes and Volkman* [1993]. All records are plotted on the same depth scale. Note the depth offset (at 14 m) by some 240–260 cm between the records of core TN057-21 and ODP Site 1089.

during spring-summer [*Ternois et al.*, 1998; *Sikes et al.*, 2005]. This calibration has subsequently been confirmed to provide reliable estimates of past summer SSTs at subantarctic to Antarctic latitudes [*Sikes et al.*, 1997; *Pichon et al.*, 1998; *Sikes et al.*, 2002, 2005].

[13] In most other oceanic areas, sediment $U^{K'}_{37}$ values have been suggested to integrate the annual temperature signal and best correlate with mean annual surface temperatures despite considerable seasonal variations in alkenone production [e.g., *Müller et al.*, 1998; *Prahl et al.*, 2005]. It may be argued that the increase in benthic grazing in response to increased primary production and organic matter flux to the seafloor [e.g., *Herguera and Berger*, 1991] annuls the dominance of alkenones produced during the seasonal flux maxima, resulting in an integrated $U^{K'}_{37}$ signal in the sediment that more uniformly reflects all seasons and hence correlates with mean annual surface temperatures [*Sachs et al.*, 2000].

[14] Moreover, regional temperature calibrations are based on limited temperature ranges and short timescales and the benefits and detriments of such calibrations compared to global calibrations are still under debate (for a review, see *Herbert* [2003]). We therefore report the SST estimates for subantarctic core MD97-2120 from the Southwest Pacific on two different SST scales using (1) the global calibration of *Prahl et al.* [1988] reflecting mean annual SSTs (outer axis in Figures 2–5) and (2) the regional Southern Ocean calibration of *Sikes and Volkman* [1993] that yields summer temperature estimates (inner axis in Figures 2–5). We use *Prahl et al.*'s [1988] calibration rather than the core-top calibration of *Müller et al.* [1998] for historical reasons and consistency with other SST reconstructions that are mainly based on the *Prahl et al.* [1988] calibration, though they result in nearly identical SSTs. For SST estimates along cores MD97-2121 and TN057-21/1089 that are both under subtropical influence (see above and Figure 1) we applied the calibration of *Prahl et al.* [1988].

[15] Present-day alkenone production in the southwest Pacific is dominated by *E. huxleyi* [*Wells and Okada*, 1997; *Bentaleb et al.*, 2002]. In the past, the relative abundance of *E. huxleyi* and Gephyrocapsa species varied with lower *E. huxleyi* contributions during glacial periods [*Wells and Okada*, 1997]. Such variations in species composition, however, do not compromise past SST reconstruction using the alkenone technique [*Müller et al.*, 1997; *Conte et al.*, 1998; *Villanueva et al.*, 2002].

[16] Alkenone fluxes in the southwest Pacific vary seasonally and differ in subtropical and subantarctic waters. North of the Chatham Rise (Subtropical Zone), flux rates are highest during midsummer and $U^{K'}_{37}$-SSTs show a cold bias relative to satellite-derived SSTs. South of the rise (Subantarctic Zone), a broad flux maximum persists from late winter to early summer, peaking in late spring, with $U^{K'}_{37}$-SSTs closely tracking measured surface temperatures [*Sikes et al.*, 2005]. The cold bias in $U^{K'}_{37}$-SSTs north of the Rise was attributed to nutrient stress and a possible contribution of alkenones produced at the base of the surface mixed layer [*Sikes et al.*, 2005]. The latter has also been

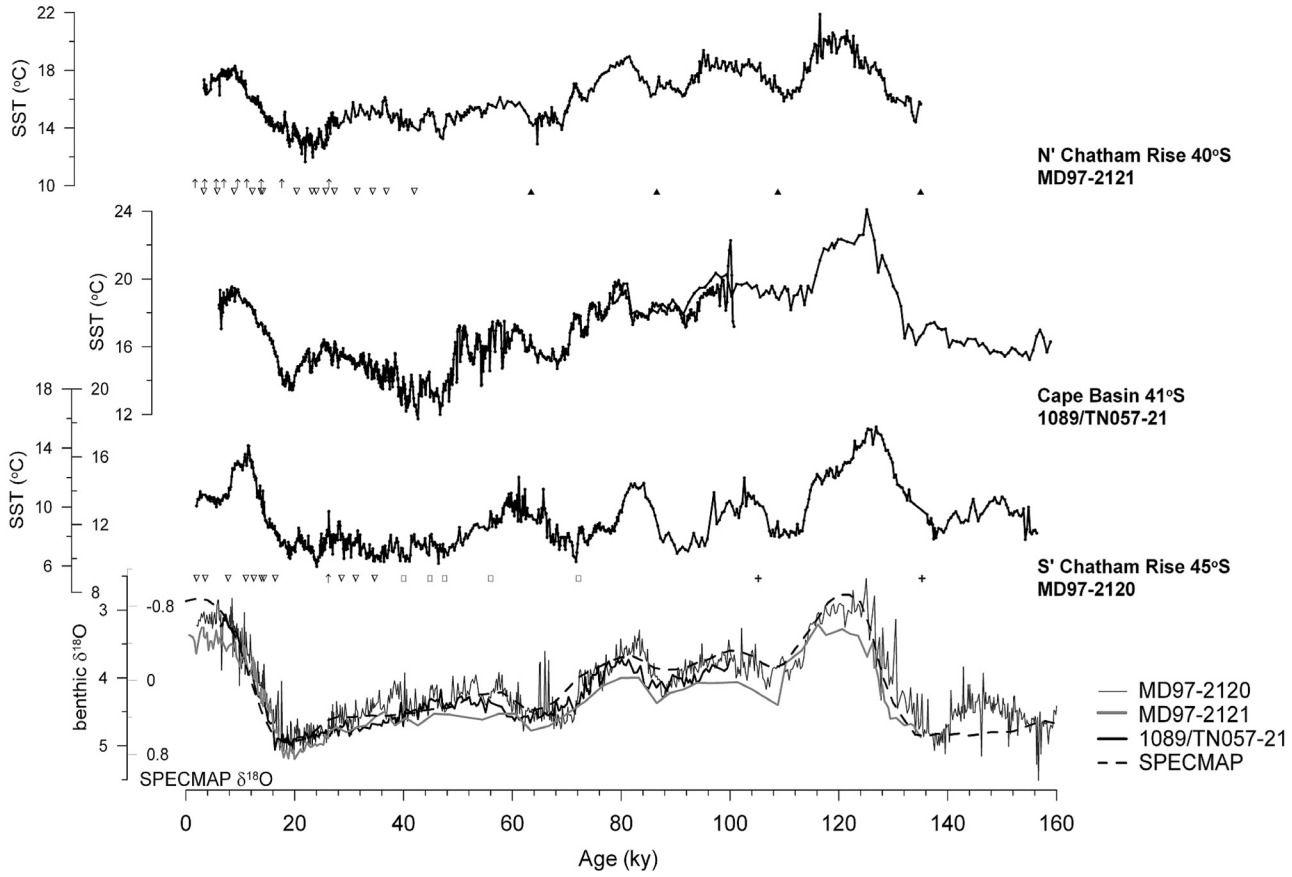

Figure 3. Alkenone SST records of cores MD97-2121, TN057/1089 and MD97-2120 plotted on their individual age scales. Symbols along the age axis denote the age control points used to construct the age models. Open triangles mark radiocarbon ages measured on foraminifera, upward arrows denote tephra layers, solid triangles are tie points used to align the benthic foraminiferal $\delta^{18}O$ records to the global benthic $\delta^{18}O$ SPECMAP stack [*Imbrie et al.*, 1993], open squares mark age tie points from aligning the benthic $\delta^{18}O$ record of core MD97-2120 to that of North Atlantic core MD95-2042 [*Shackleton et al.*, 2000], and crosses highlight ages at which the Mg/Ca-SST record of MD97-2120 was graphically aligned to the Vostok temperature record (see *Pahnke et al.* [2003] and *Pahnke and Zahn* [2005] for details). Benthic foraminiferal $\delta^{18}O$ records of all cores are shown together with the SPECMAP benthic $\delta^{18}O$ record (inner scale [*Imbrie et al.*, 1993]) in the bottom panel for relative stratigraphic control.

invoked to explain low $U^{K'}_{37}$-SSTs in the North Pacific [*Prahl et al.*, 1993; *Ohkouchi et al.*, 1999].

2.2.3. Age Models

[17] The chronology of core TN057-21-PC2, adapted from *Ninnemann and Charles* [2002], is based on visual alignment of features in the benthic $\delta^{18}O$ record and the SPECMAP benthic $\delta^{18}O$ stack [*Imbrie et al.*, 1993], and graphical tuning of the planktonic $\delta^{18}O$ record to that of well-dated nearby core RC11-83 [*Charles et al.*, 1996] (Figure 3). The age model for ODP Site 1089 is derived from visual alignment of stable oxygen isotope records to those of RC11-83 and through graphical tuning of its paleointensity record to similar records from the North Atlantic [*Hodell et al.*, 2003; *Stoner et al.*, 2003]. The stacked record TN057-21/1089 covers the past 160 kyr at a mean temporal resolution of 190 years. Mean sedimentation rates along cores TN057-21-PC2 and 1089 are 16.4 cm/kyr [*Ninnemann et al.*, 1999] and 14 cm/kyr [*Hodell et al.*, 2003], respectively.

[18] The age scale for core MD97-2120 is based on 13 ^{14}C AMS dates, a tephrochronological marker event, and visual alignment of benthic $\delta^{18}O$ and SST records to benthic $\delta^{18}O$ of North Atlantic core MD95-2042 [*Shackleton et al.*, 2000] and the Antarctic Vostok deuterium record [*Petit et al.*, 1999], respectively [*Pahnke et al.*, 2003; *Pahnke and Zahn*, 2005]. The mean temporal resolution along the 156-kyr-long record is 215 years.

[19] Core MD97-2121 was dated using a set of 9 well-dated tephra layers and 19 foraminiferal ^{14}C AMS dates [*Carter et al.*, 2002; *Carter and Manighetti*, 2006]. In the interval older than 42 kyr, the benthic $\delta^{18}O$ record was graphically aligned to the SPECMAP benthic $\delta^{18}O$ stack [*Imbrie et al.*, 1993]. The record covers the past 135 kyr at a mean temporal resolution of 196 years. Close covariation of

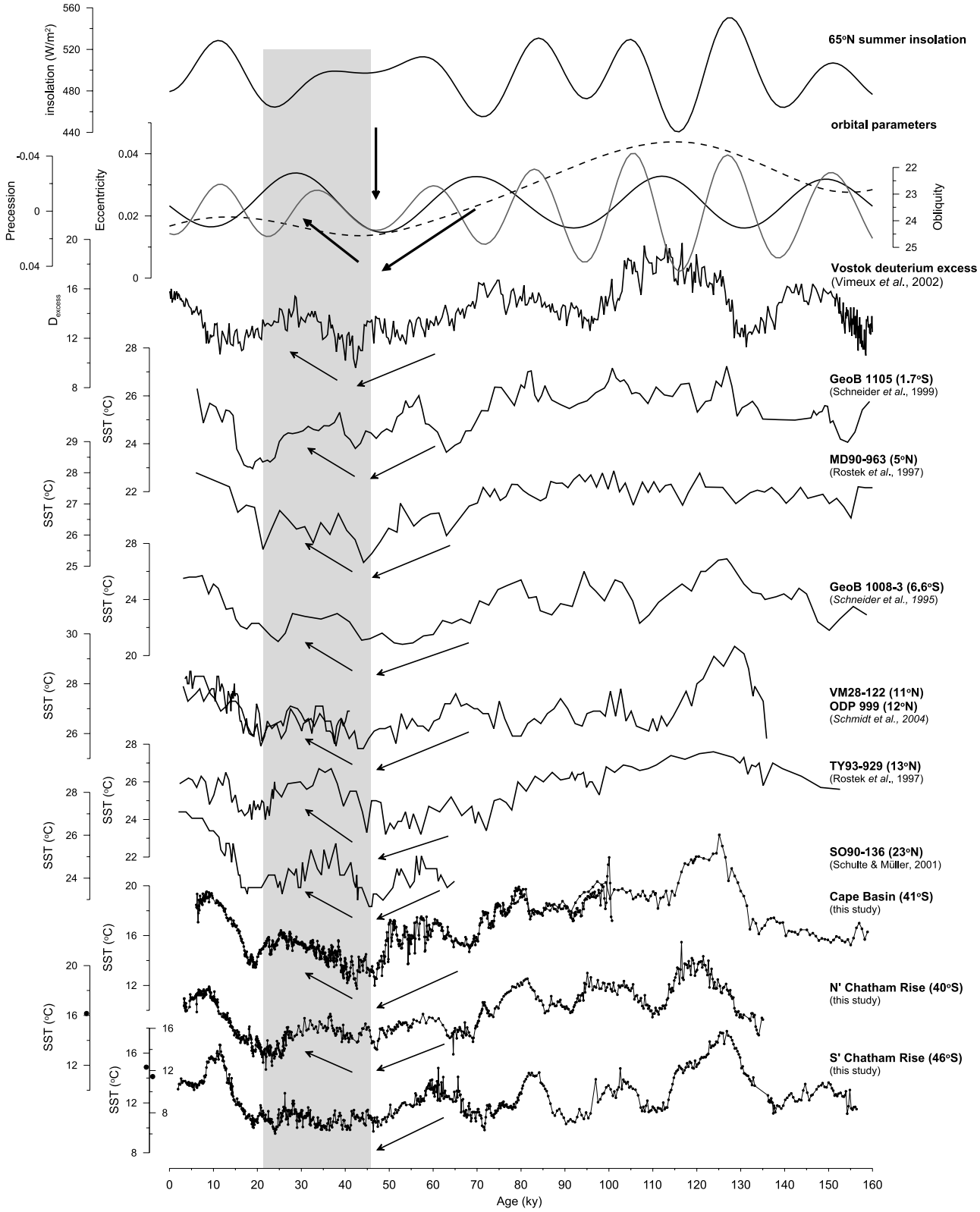
65°N summer insolation
insolation (W/m²)
orbital parameters
Precession
Eccentricity
Obliquity
Vostok deuterium excess
(Vimeux et al., 2002)
D_excess
GeoB 1105 (1.7°S)
(Schneider et al., 1999)
MD90-963 (5°N)
(Rostek et al., 1997)
GeoB 1008-3 (6.6°S)
(Schneider et al., 1995)
VM28-122 (11°N)
ODP 999 (12°N)
(Schmidt et al., 2004)
TY93-929 (13°N)
(Rostek et al., 1997)
SO90-136 (23°N)
(Schulte & Müller, 2001)
Cape Basin (41°S)
(this study)
N' Chatham Rise (40°S)
(this study)
S' Chatham Rise (46°S)
(this study)
SST (°C)
Age (ky)

Figure 4

the benthic $\delta^{18}O$ records of all three cores (Figure 3) demonstrates robustness of the individual age scales relative to each other and warrants direct comparison of their SST records.

3. Results

3.1. Core TN057-21-PC2/ODP 1089

[20] $U^{K'}_{37}$-derived SSTs along southeast Atlantic cores TN057-21/1089 range between 11.8° and 24.1°C over the past 160 kyr. Maximum SSTs occur during MIS5e, with temperatures on average 3.5°C warmer than during the early Holocene. Minimum SST values are reached at 47 and 43 kyr B.P., after which SSTs increase to 16.3°C at 25.5 kyr B.P. and then cool toward the LGM (~20 kyr B.P.). SSTs during MIS6a of 16°C are some 2°C warmer than LGM temperatures. The mean temperature changes at the penultimate and last glacial-interglacial terminations in TN057-21/1089 are 6.5° and 5.6°C, respectively.

3.2. Core MD97-2121

[21] In core MD97-2121 from the subtropical southwest Pacific, $U^{K'}_{37}$-derived SST estimates yield values between 11.7° and 21.9°C over the past 135 kyr. The record shows a gradual decrease from an early Holocene maximum (18.2°C) toward 16.8°C at the core top, dated to 3 kyr B.P. The core-top estimate deviates from satellite mean annual temperatures (~16°C) [*Uddstrom and Oien*, 1999], which may be due to the lack of recent sediments in the core.

[22] Maximum SSTs along the record occur during MIS5e with values on average 2.4°C higher than during the Holocene. Lowest SSTs are reached during the LGM. Similar to the record of TN057-21/1089, core MD97-2121 exhibits a prominent warming between 47 and 23 kyr with maximum temperatures of 16.1°C at 36.6 kyr B.P. The SST minimum of 14.4°C at 134 kyr near the base of the core is warmer by 1.1°C than the mean LGM SST of 13.3°C.

3.3. Core MD97-2120

[23] Subantarctic core MD97-2120 shows SST changes (using the calibration of *Sikes and Volkman* [1993] and of *Prahl et al.* [1988] (in parentheses)) from 9.5° to 17.8°C (6° to 16°C), with minimum and maximum temperatures at 24.12 kyr and during MIS5e, respectively. Similar to the subtropical SST records from north of Chatham Rise and from the southeast Atlantic, temperatures significantly decrease toward 47 kyr. The following temperature evolution shows no marked changes. Temperatures slightly warm toward 29–26 kyr B.P. starting at 36 kyr, and show an early temperature minimum of 9.5°C (6°C) at 24.1 kyr. Temperatures during MIS6a are some 1°C warmer than average LGM (19–22 kyr) SSTs. The core top temperature estimate using the calibration of *Sikes and Volkman* [1993] of 13.1°C underestimates present-day satellite-derived summer SSTs of 14.6°C by some 1.5°C [*Uddstrom and Oien*, 1999]. Using the calibration of *Prahl et al.* [1988] that yields mean annual temperatures, the core top SST of 10.2°C differs from satellite mean annual temperatures (11.3°C [*Uddstrom and Oien*, 1999]) by 1.1°C. The latter offset is slightly smaller, but since the last 2 kyr of the core are missing, we can not unambiguously determine which calibration provides better SST estimates.

4. Discussion

4.1. Orbital-Scale SST Variability Over the Past 160 kyr: Global Comparison

[24] The temperature pattern in our subtropical records (MC97-2121, TN057-21/1089) differs from the subantarctic (MD97-2120) SST evolution by exhibiting strong cooling at 47 kyr, warming between 47 and 23 kyr and warmer temperatures during MIS6a than during the LGM. These patterns are also in contrast to changes in global ice volume recorded by benthic foraminiferal $\delta^{18}O$ (Figure 3, bottom), that indicate gradual ice volume increase toward 20 kyr B.P., which implies global climate cooling and lowest temperatures during the LGM.

[25] An ever increasing array of paleo-SST records exists from the Atlantic, Indian and Pacific oceans [e.g., *Howard and Prell*, 1992; *Rostek et al.*, 1993; *Wells and Wells*, 1994; *Bard et al.*, 1997; *Ikehara et al.*, 1997; *Rostek et al.*, 1997; *Wells and Okada*, 1997; *Weaver et al.*, 1998; *Pelejero et al.*, 1999; *Sachs and Lehman*, 1999; *Schneider et al.*, 1999; *Lea et al.*, 2000; *Calvo et al.*, 2001a, 2001b; *Schulte and Müller*, 2001; *Cortese and Abelmann*, 2002; *Sikes et al.*, 2002; *Pahnke et al.*, 2003] and hence from a multitude of different latitudes, oceanographic settings and regional climates. Evaluation of our mid-southern latitude SST records in the context of available SST histories will thus allow us to single out local from regional temperature changes and to gain insight into latitudinal, interbasin and/or hemispheric SST variations. This comparison reveals conspicuous similarities and dissimilarities in the temperature patterns. Notably, the SST features observed primarily in our subtropical records, i.e., cooling at 47 kyr B.P., warming at 47–23 kyr B.P. and warmer SSTs during MIS6a than during the LGM, are also present in other SST records from the

Figure 4. Alkenone SST records from this study (lower panels) compared to paleo-SST reconstructions from low- to mid-latitude sites (lowest latitudes at top, higher latitude records at bottom of figure) and orbital parameters. (top to bottom) Summer insolation (21 June) at 65°N [*Laskar*, 1990]; eccentricity (dotted line), obliquity (black line) and precession (gray line) (note orientation of y axes); deuterium excess (*d*) record from Antarctica (Vostok) [*Vimeux et al.*, 2001]; SST records from East Atlantic core GeoB 1105 [*Schneider et al.*, 1999]; SST records from core MD90-963 from the Indian Ocean [*Rostek et al.*, 1997, East Atlantic core GeoB 1008 [*Schneider et al.*, 1995], the Caribbean [*Schmidt et al.*, 2004], and cores TY93-929 [*Rostek et al.*, 1997] and SO90-136KL [*Schulte and Müller*, 2001] from the Arabian Sea. Arrows mark the cooling at 47 kyr B.P. and subsequent warm anomaly, respectively. The latter is further highlighted by a shaded bar. Outer SST axis for MD97-2120 uses *Prahl et al.* [1988] calibration, inner axis uses *Sikes and Volkman* [1993]. Dots mark modern mean annual (outer axis) and summer (inner axis) satellite-derived temperatures [*Uddstrom and Oien*, 1999].

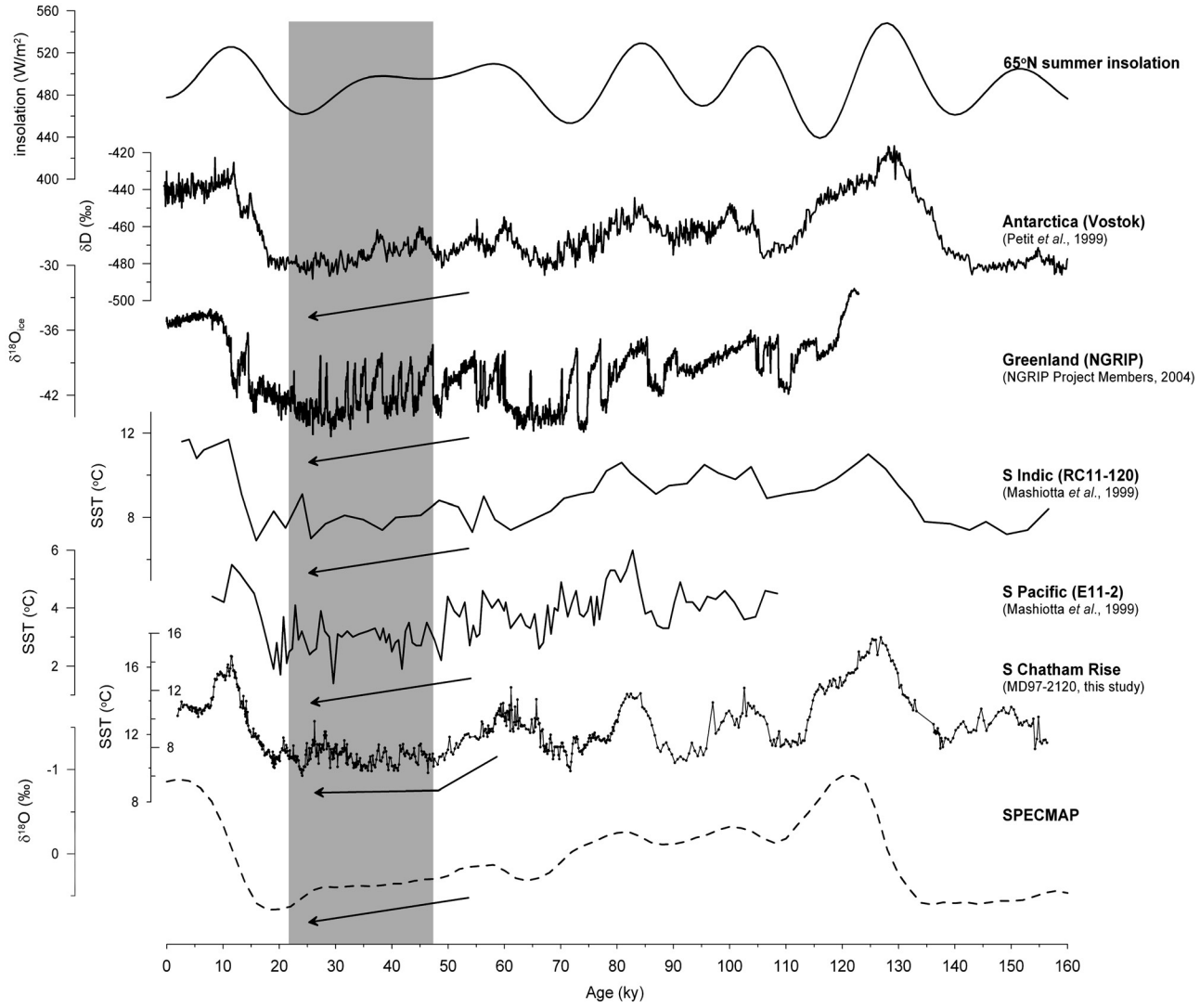

Figure 5. Paleo-temperature records from high-latitude sites compared to the alkenone SST record from subantarctic core MD97-2120 from this study. (top to bottom) summer insolation (June 21) at 65°N [*Laskar*, 1990]; Antarctic Vostok deuterium (δD) record [*Petit et al.*, 1999] on the age scale of *Shackleton* [2000]; Greenland NGRIP oxygen isotope record [*NorthGRIP Members*, 2004]; Mg/Ca-derived SST records from core RC11-120 from the subantarctic Indian Ocean [*Mashiotta et al.*, 1999] and core E11-22 from the South Pacific [*Mashiotta et al.*, 1999]; SPECMAP $\delta^{18}O$ stack taken to reflect global ice volume variations [*Imbrie et al.*, 1993].

Atlantic [e.g., *Schneider et al.*, 1995; *Villanueva et al.*, 1998; *Kirst et al.*, 1999; *Schneider et al.*, 1999; *Wolff et al.*, 1999; *Sachs et al.*, 2001; *Schmidt et al.*, 2004; *Pichevin et al.*, 2005] and Indian and Pacific oceans [e.g., *Rostek et al.*, 1993; *Emeis et al.*, 1995; *Bard et al.*, 1997; *Rostek et al.*, 1997; *Pelejero et al.*, 1999; *Herbert et al.*, 2001; *Schulte and Müller*, 2001; *Yamamoto et al.*, 2004] (see Figure 4 for some of these records and Table 2). In the Arabian Sea, three SST records (TY93-929, MD90-963, SO90-136KL) show uniform temperature changes with warmer-than-LGM SST during MIS6a, colder temperatures around 47 kyr than at the LGM and a pronounced warm anomaly at 47–23 kyr [*Rostek et al.*, 1993; *Emeis et al.*, 1995; *Rostek et al.*, 1997; *Schulte and Müller*, 2001], consistent with the SST evolution observed in our subtropical records. Considering the contrasting monsoon influences and past monsoon variations at the core sites in the Arabian Sea, as documented by upwelling proxies such as *Globigerina bulloides* abundances, alkenone concentrations and organic carbon concentrations [*Rostek et al.*, 1993; *Emeis et al.*, 1995; *Schulte et al.*, 1999], it has been suggested that the recorded temperature changes are not affected by variations in monsoon activity [*Emeis et al.*, 1995; *Schulte et al.*, 1999; *Schulte and Müller*, 2001]. Similar temperature changes are also documented in alkenone SST records from off the Somalian coast (MD85-668, MD85-674) [*Bard et al.*, 1997] and in a faunal SST record from the southwest Indian Ocean (MD97-254) [*van Campo et al.*, 1990]. All three records

Table 2. Location and Source of SST Records Shown in Figure 6[a]

Number	Core	Longitude, °W	Latitude, °N	Water Depth, m	Region	SST Proxy	Reference
			Records Showing Tropical Temperature Pattern				
1	GRIP	37.63	72.58		Greenland	D-excess	*Masson-Delmotte et al.* [2005]
2	SU90-08	30.4	43.5	3100	N Atlantic	$U^{K'}_{37}$	*Villanueva et al.* [1998]
3	MD01-2421	−141.78	36.03	2224	NW Pacific	$U^{K'}_{37}$	*Yamamoto et al.* [2004]
4P	ODP 1012	118.28	32.38	1783	California Current	$U^{K'}_{37}$	*Herbert et al.* [2001]
5	SO90-136KL	−66.5	23.12	568	Arabian Sea	$U^{K'}_{37}$	*Schulte and Müller* [2001]
6	ODP 723A	−57.62	18.05	816	Arabian Sea	$U^{K'}_{37}$	*Emeis et al.* [1995]
7P	17954	−111.53	14.8	1520	S China Sea	$U^{K'}_{37}$	*Pelejero et al.* [1999]
8	TY93929/P	−53.25	13.7	2490	Arabian Sea	$U^{K'}_{37}$	*Rostek et al.* [1997]
9	ODP 999A	78.73	12.75	2827	Caribbean	Mg/Ca	*Schmidt et al.* [2004]
10	VM28-122	78.42	11.57	3623	Caribbean	Mg/Ca	*Schmidt et al.* [2004]
11	17961	−112.33	8.5	1968	S China Sea	$U^{K'}_{37}$	*Pelejero et al.* [1999]
12	MD90-963	−73.88	5.07	2446	Indian Ocean	$U^{K'}_{37}$	*Rostek et al.* [1997]
13	GeoB1523	41.62	3.83	3292	NW Atlantic	foraminifera	*Wolff et al.* [1999]
14,P	ODP 846	90.82	3.08		E Pacific	$U^{K'}_{37}$	*Liu and Herbert* [2004]
15	MD85-674	−50.43	3.07	4875	Indian Ocean	$U^{K'}_{37}$	*Bard et al.* [1997]
16	MD85-668	−46.03	0	4020	Indian Ocean	$U^{K'}_{37}$	*Bard et al.* [1997]
17	GeoB1105	12.43	−1.67	3225	Benguela Current	$U^{K'}_{37}$, forams	*Schneider et al.* [1999]
18	GeoB1008-3	−10.32	−6.58	3124	Angola Basin	$U^{K'}_{37}$	*Schneider et al.* [1995]
19,P	GeoB1016-3	−11.68	−11.77	3411	Angola Basin	$U^{K'}_{37}$	*Schneider et al.* [1995]
20	MD79-254	−38.67	−17.89	1934	SW Indian Ocean	foraminifera	*van Campo et al.* [1990]
21,P	GeoB1028-5	−9.19	−20.1	2209	Angola Basin	$U^{K'}_{37}$	*Schneider et al.* [1995]
22	GeoB1712-4	−12.81	−23.32	998	Benguela Current	$U^{K'}_{37}$	*Kirst et al.* [1999]
23	MD97-2121	−177.99	−40.38	3014	N Chatham Rise	$U^{K'}_{37}$	this study
24,P	GeoB1710	11.7	−23.43	2987	Benguela Current	$U^{K'}_{37}$	*Kirst et al.* [1999]
25	ODP 1089	−9.89	−40.94	4621	Cape Basin	$U^{K'}_{37}$	*Sachs et al.* [2001]; this study
26	TN057-21	−7.82	−41.13	4981	Cape Basin	$U^{K'}_{37}$	*Sachs and Anderson* [2003]
27	R657	−179.5	−42.5	1408	N Chatham Rise	$U^{K'}_{37}$, forams	*Sikes et al.* [2002]
28	Vostok	−106.38	−79		Antarctica	D-excess	*Vimeux et al.* [2002]
			Records Showing High-Latitude Temperature Pattern				
29	NGRIP	41.7	76.2		Greenland	$\delta^{18}O$	*NorthGRIP Members* [2004]
30	GISP2	37	72.7		Greenland	$\delta^{18}O$	*Grootes and Stuiver* [1997]
31	BOFS16K	23	59	2370	N Atlantic	$U^{K'}_{37}$, faunal	*Weaver et al.* [1999]
32	RC11-120	−79.87	−43.52	3135	subant. Indian	Mg/Ca	*Mashiotta et al.* [1999]
33	U939	−179.5	−44.5	1300	S Chatham Rise	$U^{K'}_{37}$	*Sikes et al.* [2002]
34	U938	−179.5	−45.1	2700	S Chatham Rise	$U^{K'}_{37}$	*Sikes et al.* [2002]
35	MD97-2120	−174.93	−45.53	1210	S Chatham Rise	$U^{K'}_{37}$	this study
36	DSDP 594	−174.95	−45.52	1204	S Chatham Rise	foraminifera	*Wells and Okada* [1997]
37	E49-17,21,23	−90.3 to −95	−42.2 to −48	~3300	SE Indian Ocean	radiolaria	*Morley* [1989]
38	PS1768-8	−4.48	−52.59	3299	S Atlantic	diatoms	*Zielinski et al.* [1998]
39	E11-2	115.08	−56.07	3094	subant. Pacific	Mg/Ca	*Mashiotta et al.* [1999]
40	Vostok	−106.38	−79		Antarctica	δD	*Petit et al.* [1999]
			Low-/Mid-Latitude Records Showing High-Latitude Temperature Pattern				
41	ODP 1020	126.43	41	3042	California Current	$U^{K'}_{37}$	*Herbert et al.* [2001]
42	MD95-2040	9.86	40.58	2465	Iberian Margin	$U^{K'}_{37}$	*Pailler and Bard* [2002]
43	MD95-2042	10.17	37.8	3146	Iberian Margin	$U^{K'}_{37}$	*Pailler and Bard* [2002]
44	MD95-2037	32.03	37.08	2630	N Atlantic	$U^{K'}_{37}$	*Calvo et al.* [2001a, 2001b]
45	SU94-20bk	16.65	25	1445	NE Atlantic	$U^{K'}_{37}$	*Sicre et al.* [2000]
46	La Paz 21P	109.47	22.99	624	California Current	$U^{K'}_{37}$	*Herbert et al.* [2001]
47	ODP 658C	18.35	20.45	2263	NE Atlantic	$U^{K'}_{37}$	*Zhao et al.* [1995]
48	BOFS31/1K	20.16	19	3300	NE Atlantic	$U^{K'}_{37}$	*Zhao et al.* [1995]
49	MD97-2141	−121.3	8.8	3633	South China Sea	Mg/Ca	*Dannenmann et al.* [2003]
50	TR163-19	90.95	2.26	2348	Cocos Ridge	Mg/Ca	*Lea et al.* [2000]
51	W8402A-14	138.96	0.95	4287	Pacific	$U^{K'}_{37}$	*Jasper et al.* [1994]
52	ODP 806B	−159.36	0.32	2520	Ontong Java Pl.	Mg/Ca	*Lea et al.* [2000]
53	GeoB1711-4	−12.38	−23.3	1967	Benguela Current	$U^{K'}_{37}$	*Kirst et al.* [1999]
54	ODP 1089	−9.89	−40.94	4621	Cape Basin	radiolaria	*Cortese et al.* [2004]

[a]P in first column denotes records showing only part of the low-/mid-latitude temperature pattern (see text).

show cooling toward 47 kyr B.P., with the South Indian core reaching lower temperatures than during the LGM, and a warm interval between 47 and 20 kyr that is terminated by a drop to LGM temperatures. Two SST records derived from Mg/Ca ratios in planktonic foraminifera suggest Caribbean surface waters also warmed between 45 and 20 kyr B.P. (ODP 999, VM28-122) and experienced cooling at 45 kyr B.P. (VM28-122) [*Schmidt et al.*, 2004]. The same patterns are also present in several cores from the low- to mid-latitude southeast Atlantic (cores GeoB 1105, GeoB 1008-3, GeoB 1016-3) [*Schneider et al.*, 1995; *Kirst et al.*, 1999; *Schneider et al.*, 1999] (for a more extensive listing of records, see Table 2).

[26] Some $U^{K'}_{37}$-SST records from nearby core sites (GeoB 1028-5, GeoB 1710), however, lack the prominent warm

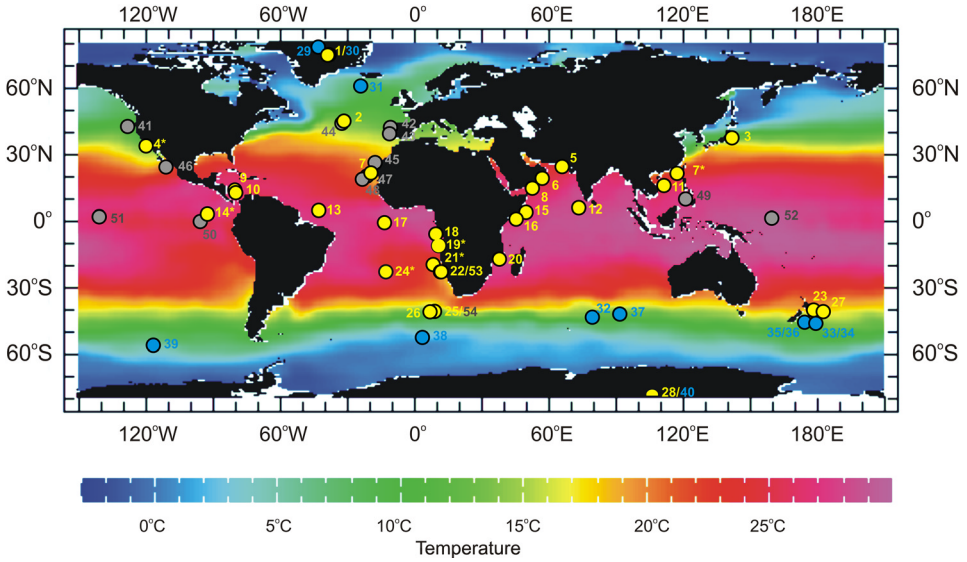

Figure 6. Locations of cores showing a low- to mid-latitude temperature pattern (yellow) and high-latitude SST signal (blue). Sites of low-/mid-latitude SST records that show a temperature pattern more similar to that at high latitudes are marked by gray symbols. Asterisks mark records that show only part of the low-/mid-latitude temperature pattern. The map shows January–March SST distributions from the *Levitus and Boyer* [1994] atlas. Locations, proxies, and references for all cores are listed in Table 2.

anomaly at 47–23 kyr documented in SST profiles described above but exhibit higher temperatures during MIS6a than during the LGM and cooling toward ~47 kyr B.P. [*Schneider et al.*, 1995, 1999]. $U^{K'}_{37}$-SST values in some records from the tropical and subtropical Atlantic and Pacific [*Villanueva et al.*, 1998; *Herbert et al.*, 2001; *Liu and Herbert*, 2004] are higher during MIS6a than during the LGM but decrease toward the LGM without a marked warming during MIS3 (Table 2). A sea surface temperature record from 17°S in the southeast Pacific (TG7) likewise shows temperatures during MIS6a that exceed those of the LGM, but is devoid of substantial changes on timescales <100 kyr [*Calvo et al.*, 2001a].

[27] We note that a large part of the low- and mid-latitude SST records shown in Figures 4 and 6 are from upwelling areas. This could introduce local temperature variability and obscure the regional climatic imprint on SST [e.g., *Pichevin et al.*, 2005]. However, several of the records mentioned above, including those from the Caribbean [*Schmidt et al.*, 2004], the central South Atlantic [*Schneider et al.*, 1999], the Indian Ocean [*Rostek et al.*, 1997] and the new records presented in this study, are from areas not directly influenced by upwelling, making us confident that the consistent SST patterns are not primarily caused by upwelling dynamics.

[28] Our subantarctic SST record (MD97-2120), on the other hand, shows more similarities with the benthic $\delta^{18}O$ record and several $U^{K'}_{37}$-SST records from high latitudes in the South Indian Ocean (core RC11-120 [*Mashiotta et al.*, 1999]), the South Pacific (core E11-2 [*Mashiotta et al.*, 1999]; cores U939, U938 [*Sikes et al.*, 2002]), northeast Pacific (ODP Site 1020 [*Herbert et al.*, 2001]), the North Atlantic (core MD95-2040 [*Pailler and Bard*, 2002]) and the climate records from Greenland and Antarctic ice cores (e.g., GISP2, Vostok, EPICA [*Grootes and Stuiver*, 1997; *Petit et al.*, 1999; *EPICA Community Members*, 2004]) (see also Table 2). The long-term gradual cooling from ~60 kyr B.P. to the LGM, recorded in these records, as well as similar temperatures during MIS6a and MIS2 are features of the global ice volume record documented by benthic $\delta^{18}O$ (Figure 5). They are, however, distinctly different from the temperature evolution in our subtropical cores and other mid- to low-latitude SST records described above.

[29] In the North Atlantic, surface ocean records often show a dominant millennial-scale pattern associated with the episodic discharge of icebergs from the Northern Hemisphere ice sheets that complicate the identification of longer-term features [e.g., *Chapman et al.*, 1996; *Madureira et al.*, 1997; *Sachs and Lehman*, 1999; *Bard et al.*, 2000; *Bard*, 2002]. Other high-latitude SST records from the Sea of Okhotsk [*Seki et al.*, 2004] and the Sea of Japan [*Ishiwatari et al.*, 2001] show anomalously warm temperatures during the LGM, which has been ascribed to the isolation of these areas from the open ocean during times of lower sea level; that is, these records likely reflect very localized SST changes.

[30] The "anomalous" glacial temperature pattern in our subtropical cores is observed in many alkenone SST records from low and mid latitudes (Figures 4 and 6 and Table 2), implying a wide geographic footprint. The glacial SST pattern we observe in our subantarctic core south of the Chatham Rise tracks global ice volume changes as recorded by benthic foraminiferal $\delta^{18}O$ and appears to be characteristic of SST records from subpolar and polar latitudes of both hemispheres (Figures 5 and 6 and Table 2). Disappearance of the "low-/mid-latitude temperature signal" in core MD97-2120 just 5° in latitude south of core MD97-2121 may be due to the strong hydrographic front of the Subtropical Front that marks the transition from subtropical to subantarctic waters and therefore amplifies the separation

of the low-/mid- and high-latitude temperature patterns (Figure 1).

[31] A number of SST records from low to mid latitudes do not show the temperature pattern described above (see Table 2) and instead more closely follow the ''high-latitude'' pattern. Different paleo-SST proxies (e.g., planktonic foraminiferal Mg/Ca, faunal assemblage structure, $U^{K'}_{37}$) often show considerable differences in both absolute values and variability along records [e.g., *Sikes and Keigwin*, 1994; *Chapman et al.*, 1996; *Sikes and Keigwin*, 1996; *Weaver et al.*, 1999; *Sikes et al.*, 2002]. This can also be seen in the South Atlantic core studied here (TN057-21/1089), where the $U^{K'}_{37}$-derived SST record differs from a temperature record based on radiolarian assemblages [*Cortese and Abelmann*, 2002]. Such differences are usually explained by invoking differences in water column and/or seasonal temperatures reflected by the proxies, or differences in sensitivity to other environmental factors (e.g., carbonate dissolution affects Mg/Ca and faunal SST estimates, while alkenone unsaturation ratios are unaffected [*Thunell and Honjo*, 1981; *Brown and Elderfield*, 1996]). Faunal assemblage structures are further prone to variations in thermocline depth and nutrient concentrations that can mask actual temperature variations [*Watkins and Mix*, 1998]. Nutrient or light limitation has been shown to cause $U^{K'}_{37}$-SST biases toward lower and higher temperatures, respectively [*Prahl et al.*, 1993; *Epstein et al.*, 1998]. Moreover, alkenones attach to fine particles and are therefore more sensitive to sediment transport than sand-sized foraminifera, which can result in temporal and absolute temperature offsets between $U^{K'}_{37}$- and foraminifera-derived estimates [*Bard*, 2001; *Ohkouchi et al.*, 2002; *Mollenhauer et al.*, 2003]. Despite these potential effects on alkenone SST reconstructions, the similarities in low-/mid-latitude SST patterns at core sites influenced by different oceanic and sedimentary conditions suggest that our $U^{K'}_{37}$-SST records and those shown in Figures 4 and 5 and listed in Table 2, primarily reflect changes in sea surface temperature. Moreover, given the above-mentioned difficulties with different SST proxies, the correlation of some SST records from tropical and subtropical latitudes with high-latitude temperatures does not compromise our interpretation that the ''anomalous'' SST pattern in our subtropical cores is a prevailing low- to mid-latitude feature that is not found at latitudes poleward of ~43°N/S.

4.2. Mid-/Low- Versus High-Latitude SST Variability Over the Past 160 kyr

[32] The new mid-southern latitude SST records from the southwest Pacific and southeast Atlantic presented here indicate significant deviations from changes in global ice volume and the temperature evolution at high latitudes on orbital timescales. This is unexpected with respect to the principal notion that the Late Quaternary temperature and climate pattern follows global ice volume variations as recorded in benthic foraminiferal $\delta^{18}O$. However, the clear recurrence of this deviation in other SST records reveals this ''anomaly'' as common feature of low to mid latitudes, suggesting a differential temperature response at low/mid and high latitudes.

[33] In considering possible causes for these different SST trends at high and low/mid latitudes we focus on insolation as possible external climate driving force because it (1) varies meridionally and (2) has a timescale of variations similar to the SST trends we observe.

4.2.1. Temperature Changes During Late MIS3: Potential Driving Forces

[34] The late-MIS3 warm anomaly in our subtropical South Pacific and South Atlantic SST records that is also present in other SST records from low and mid latitudes, occurred in the middle of the last glacial period when polar ice sheets were still growing [*Imbrie et al.*, 1993; *Schrag et al.*, 2002] and high-latitude temperatures decreasing toward that LGM temperature minimum [e.g., *Grootes and Stuiver*, 1997; *Mashiotta et al.*, 1999; *Petit et al.*, 1999]. The classic Milankovitch climate driving force, i.e., summer insolation at 65°N, was relatively high throughout MIS3, with only a small drop at 47 kyr B.P., and gradually decreased during the time of the low-/mid-latitude SST warm anomaly toward a minimum at ~20 kyr B.P. (Figure 4). The temperature pattern observed in tropical to temperate oceanic regions can therefore not be explained by a direct response of the surface ocean to Northern Hemisphere summer insolation. Instead, the observed cooling at 47 kyr B.P. and following SST warm anomaly coincide with obliquity and precession maxima and minima, respectively (Figure 4). Obliquity causes in-phase mean annual insolation changes between ~43°N and S and opposite phasing poleward of ~43°N/S. Low obliquity therefore results in increased insolation equatorward of 43°N/S and decreased insolation poleward of 43°N/S, and vice versa [*Loutre et al.*, 2004]. This 180°-phase shift in obliquity-driven mean annual insolation changes near 43°N/S and a response of ocean temperatures to mean annual insolation forcing would be consistent with the opposing SST trends observed here between records from low/mid (<~43°N/S) and high latitudes (>~43°N/S).

[35] Several other influences of obliquity on climate are conceivable. First, changes in winter insolation at high latitudes are dominated by obliquity as the tilt angle of the Earth's axis determines whether high latitudes receive insolation during winter or not. However, it is evident that insolation close to zero (winter insolation at high latitudes) will have a very limited effect on temperature changes and is thus unlikely to have significantly contributed to past climatic changes. Second, the insolation gradient between different latitudes closely varies with obliquity and has been suggested to exert a major influence on moisture transport to high latitudes and hence snow accumulation at the poles [*Raymo and Nisancioglu*, 2003]. The resulting ice albedo feedback would influence global climates, providing a possible explanation for the dominant 41-kyr period in climate records prior to ~900 kyr B.P. [*Raymo and Nisancioglu*, 2003]. However, an almost exclusively obliquity-driven variation in insolation gradients is only achieved between narrow latitude bands, for example, between 65°N and 30°N June insolation. Moreover, while insolation gradients may account for changes in the source area of moisture that is transported to the poles and the vigor of this transport (see below and *Vimeux et al.* [2002]), they cannot explain the differential temperature patterns observed at

low/mid and high latitudes. Finally, as discussed above, mean annual insolation at all latitudes exclusively varies with obliquity and is symmetric about the equator with a phase shift at ~43°N/S. These insolation changes are small at low to mid latitudes with amplitudes of 0.6 W/m^2 (40°N/S) to 3.6 W/m^2 (0°). However, as the upper ocean integrates the insolation signal over several years, mean annual insolation changes may have a significant impact on variations in sea surface temperature. Moreover, low- to mid-latitude warming may have been reinforced by local greenhouse effects caused by increased water vapor and cloud formation over warm ocean areas [e.g., *Hallberg and Inamdar*, 1992; *Gupta et al.*, 1996]. *Pierrehumbert* [1999] suggested that this mechanism may be active despite the negative feedback of radiative cooling caused by increased cloud cover, because it is compensated for by additional heating through adiabatic compression due to subsidence in the subtropics and latent heat release in convective areas. Such feedback mechanisms suggest that mean annual insolation changes may constitute an important contributing driving force to the observed temperature evolution at the end of MIS3.

[36] In contrast to mean annual insolation changes that are exclusively driven by obliquity variations, daily insolation in the tropics is dominated by orbital precession and is therefore of opposite phasing about the equator [*Berger et al.*, 1993]. As mentioned above and shown in Figure 4, the late-MIS3 warm anomaly in tropical and subtropical SST records coincides with a minimum in precession and hence with a maximum in Northern Hemisphere summer insolation, but a minimum in Southern Hemisphere summer insolation. The consistency of this pattern in both hemispheres suggests that it is unlikely to be a response to local daily insolation forcing and rather caused by the interaction of relatively weak mean annual insolation forcing with global, i.e., 65°N summer insolation forcing. The eccentricity minimum at this time may have been instrumental in increasing the contribution of obliquity-driven mean annual insolation to climate forcing by dampening the precessional amplitude (see Figure 4). Small changes in precession implicate weak seasonal modulation of insolation and hence a reduced effect of those changes on climate. These conditions may have enhanced the response of sea surface temperatures to variations in mean annual insolation at low/mid latitudes.

[37] The most striking examples for obliquity signals in climate records from the Late Quaternary are the deuterium excess records from Antarctica [*Vimeux et al.*, 1999, 2001, 2002] and Greenland [*Masson-Delmotte et al.*, 2005]. Deuterium excess (d) reflects moisture source temperatures, suggesting the d variability in polar ice mirrors SST changes in the main moisture source areas, the low to mid latitudes, or it is an expression of spatial changes in moisture source and subsequent transport to high latitudes in response to changing meridional temperature gradients. Another example is surface temperature and salinity changes in the North Atlantic that show opposing trends north and south of ~43°N during MIS5, in line with a dominant response to obliquity-driven mean annual insolation changes [*Cortijo et al.*, 1999]. A recent analysis suggests that the timing of Pleistocene deglaciations is consistent with forcing by every second or third obliquity maximum [*Huybers and Wunsch*, 2005]. The authors propose that obliquity maxima, by increasing high-latitude insolation, may increase basal ice sheet temperatures and lead to melting of thick ice sheets. Alternatively, as suggested by *Johnson* [1991] for the penultimate deglaciation, the lowered meridional insolation gradient during obliquity maxima may have led to a reduction in poleward moisture transport and hence starved high-latitude ice sheets of precipitation. These studies demonstrate the potentially crucial impact of obliquity variations on climate.

[38] Dominant precession signals have been reported from several low-latitude climate records and suggested to reflect a response to the precession-driven part of Northern Hemisphere summer insolation [e.g., *Perks et al.*, 2002] or local daily insolation [*Baker et al.*, 2001; *Bush et al.*, 2002; *Cruz et al.*, 2005]. Orbital configurations similar to that during MIS3 with minima in eccentricity, obliquity and precession also occurred during MIS6 (~150 kyr B.P.) and 8 (~260 kyr B.P.). But eccentricity values were lower around 45 kyr B.P. than during the two earlier glacial periods. The paleoclimatic evidence for these periods is considerably more ambiguous and sparser, as fewer records cover these periods. Records showing a clear and pronounced warming at the end of MIS6 include our record from south of Chatham Rise (Figure 4) and two records from the North Atlantic at 40°N (MD95-2042, MD95-2040 [*Pailler and Bard*, 2002]) and 43.5°N [*Villanueva et al.*, 1998] and the southeast Atlantic [23°S, *Kirst et al.*, 1999]. Several records from the low/mid latitude Atlantic (GeoB1016-3, 1105, 1710 [*Schneider et al.*, 1999]; GeoB112 [*Nürnberg et al.*, 2000] (and the tropical Pacific (TR163-10, ODP Site 806 [*Lea et al.*, 2000]) show a small positive temperature departure, while other SST records, for example, from the Atlantic (GeoB1008 [*Schneider et al.*, 1995]) and the North Indian Ocean (MD90-963 [*Rostek et al.*, 1997]), exhibit no discernable warm anomaly at this time. Only a few records exist that extend to or beyond MIS8. A clear sea surface warming is documented in the Mg/Ca-derived SST record from subantarctic Pacific core MD97-2120 [*Pahnke et al.*, 2003], and in the alkenone-SST record from tropical Atlantic core GeoB1105 [*Schneider et al.*, 1999]. Alkenone-SST records from the northeast Pacific (La Paz 21P and ODP Site 1012 [*Herbert et al.*, 2001]) and Mg/Ca-derived SST records from the tropical Pacific (TR163-19 and ODP Site 806 [*Lea et al.*, 2000]), on the other hand, do not exhibit a temperature anomaly.

[39] Similar to the warm excursion during MIS3, the MIS6 SST anomaly would be in line with mean annual insolation forcing presumably in combination with a surface ocean response to the precession-driven increase in Northern Hemisphere summer insolation (Figure 4). The presence of this temperature excursion in core MD97-2120 south of Chatham Rise may indicate the transitional position of this site between mid- and high-latitude climate impacts.

4.2.2. Long-Term SST Evolution Over the Past 160 kyr

[40] Higher temperatures during MIS6a than during the LGM and the long-term temperature evolution seen in many

paleo-SST records from low/mid latitudes show similar timing and amplitudes as Earth's orbital eccentricity trend. The 100-kyr period of eccentricity is modulated by the 400-kyr cycle of eccentricity, resulting in lowest values since the past ~350 kyr at the time of the 47-kyr SST minimum and subsequent warm anomaly. While the effect of eccentricity changes on insolation is negligible, eccentricity modulates the amplitude of precession and hence the seasonal insolation contrast. With precession being the dominant orbital parameter influencing daily insolation changes at low latitudes, eccentricity may have contributed to low-/mid-latitude climate changes through its impact on the amplitude of precession. In contrast, high-latitude insolation changes are less affected by precession, which may explain why high-latitude temperatures during MIS6 were similar to those during the previous and following glacials and hence relatively colder than at low and mid latitudes. Eccentricity imprints on SST changes have previously been described from tropical and subtropical Atlantic sites [*Schneider et al.*, 1999] and east Pacific paleo-records [*Calvo et al.*, 2001a].

4.3. Implications for Meridional Temperature Gradients and Global Climate Variations

[41] The distribution of paleo-SST records with contrasting temperature patterns indicates differential heating between low/mid and high latitudes (Figures 4, 5, and 6) and suggests an increase in the meridional thermal gradient at 47–23 kyr B.P. For such conditions, the thermal wind balance predicts stronger winds [*Peixoto and Oort*, 1992] and thus enhanced atmospheric transport of heat and moisture from low to high latitudes. Momentum conservation requires an increase in westerly wind strength and zonal surface ocean circulation in response to increased poleward atmospheric and ocean transport. A resulting sharpening of thermal oceanic fronts at the subtropical-subpolar boundary has been shown to have a positive feedback on atmospheric temperature gradients [*Cessi*, 2000] and may have reinforced the disparate SST pattern at the end of MIS3.

[42] Invigorated meridional circulation in both atmosphere and ocean may have resulted in increased moisture transport from the warm low/mid latitudes to the cold polar regions. The modern moisture sources for Antarctic and Greenland precipitation are the mid-southern latitude oceans [*Delaygue et al.*, 2000; *Reijmer et al.*, 2002] and the mid- to high-latitude North Atlantic and Pacific oceans [*Charles et al.*, 1994], respectively. A model simulation [*Delaygue et al.*, 2000] and the deuterium excess records from Antarctica [*Vimeux et al.*, 1999, 2001] suggest that the low-latitude moisture contribution to Antarctica slightly increased during the LGM at the expense of the high-latitude source as a result of steeper meridional temperature gradients. This highlights the importance of the low/mid latitudes as moisture supplier for continental ice sheets today as well as during glacial times. Enhanced ice accumulation due to increased moisture supply may have increased high-latitude cooling through ice albedo and altitude feedbacks. In turn, lower high-latitude temperatures would have led to tundra expansion at the expense of forests, further increasing the albedo effect and amplifying cooling [e.g., *Gallimore and Kutzbach*, 1996]. A low- to mid-latitude moisture source and increased poleward moisture transport may therefore be the key to sustained ice accumulation at times of high-latitude cooling.

[43] Using an ocean-atmosphere coupled model, *Khodri et al.* [2001] simulated climate conditions at the last glacial inception (115 kyr B.P.) and suggested that enhanced equator-to-pole thermal gradients induced by seasonal perturbations in insolation forcing led to an increase in northward heat and moisture transport. Similar dynamics may have been active just prior to the LGM owing to differential heating of high and low/mid latitudes. Simple box models of the climate system also suggest a critical role for changes in sea-ice extent, through its albedo and insulating effects, in regulating high-latitude precipitation and ice accumulation [*Gildor and Tziperman*, 2000, 2001]. With Milankovitch forcing incorporated into the model, midlatitude atmospheric and ocean temperatures directly respond to insolation changes, while high-latitude climate variables rather respond to changes in ice mass balance [*Gildor and Tziperman*, 2000]. Our SST observations would be in line with such scenario in that low- to mid-latitude temperatures follow obliquity-driven mean annual insolation changes and precession-modulated Northern Hemisphere summer insolation, while high-latitude temperatures decreased in concert with increasing global ice volume.

5. Conclusions

[44] Three alkenone records from the midlatitude Southern Hemisphere document SST variability over the past 160 kyr and thus the last interglacial period to the present. Two of these records that document subtropical temperature variability in the southwest Pacific and southeast Atlantic reveal coherent temperature patterns that deviate significantly from changes in global ice volume and the temperature evolution at high northern and southern latitudes. Most notably, subtropical temperatures were higher during MIS6a compared to the LGM, anomalously low at 47 kyr and warmed 47–23 kyr B.P., when high latitudes cooled and global ice volume increased. Comparison with other available paleo-SST records indicates that these patterns are a consistent feature of low to mid latitudes in both hemispheres. This "anomalous" temperature evolution is consistent with a response of sea surface temperature to mean annual insolation changes that are exclusively driven by obliquity and have the same phasing in this latitude band (<43°N/S). Temperature changes at high latitudes, on the other hand, more closely follow the global ice volume evolution as recorded in benthic foraminiferal $\delta^{18}O$. These differential temperature changes between low/mid and high latitudes imply an increase in the meridional thermal gradient during the last glacial that may have resulted in enhanced moisture transport to high latitudes. Increased moisture supply to the poles may have been instrumental in sustaining and promoting continued ice sheet growth during the last glacial period culminating in maximum ice extent and high latitude cooling ~20 kyr B.P. This highlights the role of the low to mid latitudes in the global climate system and emphasizes their potential as important players in the ice-age cycles of the Late Quaternary.

[45] **Acknowledgments.** We are grateful to Barbara Manighetti and Lionel Carter (Wellington, New Zealand) for providing sediment samples, the age model, and the benthic oxygen isotope data from core MD97-2121. Ying Chang and Maria Schriver assisted with alkenone analyses. We thank Eva Calvo and an anonymous reviewer for helpful comments that improved the manuscript. Funding for this research was provided in part by the Gary Comer Science and Education Foundation (J. P. S.), the Jeptha H. and Emily V. Wade Award for Research (J. P. S.), and a Henry L. and Grace Doherty Professorship (J. P. S.).

References

Baker, P. A., C. A. Rigsby, G. O. Seltzer, S. C. Fritz, T. K. Lowenstein, N. P. Bacher, and C. Veliz (2001), Tropical climate changes at millennial and orbital timescales on the Bolivian Altiplano, *Nature*, *409*, 698–701.

Bard, E. (2001), Comparison of alkenone estimates with other paleotemperature proxies, *Geochem. Geophys. Geosyst.*, *2*, doi:10.1029/2000GC000050.

Bard, E. (2002), Abrupt climate changes over millennial time scales: Climate shock, *Phys. Today*, *55*, 32–38.

Bard, E., F. Rostek, and C. Sonzogni (1997), Interhemispheric synchrony of the last deglaciation inferred from alkenone palaeothermometry, *Nature*, *385*, 707–710.

Bard, E., F. Rostek, J. L. Turon, and S. Gendreau (2000), Hydrological impact of Heinrich events in the subtropical northeast Atlantic, *Science*, *289*, 1321–1324.

Bentaleb, I., M. Fontugne, and L. Beaufort (2002), Long-chain alkenones and $U^{K'}_{37}$ variability along a south-north transect in the Western Pacific Ocean, *Global Planet. Change*, *34*, 173–183.

Berger, A., M. F. Loutre, and C. Tricot (1993), Insolation and Earth's orbital periods, *J. Geophys. Res.*, *98*, 10,341–10,362.

Brassell, S. C., G. Eglinton, I. T. Marlowe, U. Pflaumann, and M. Sarnthein (1986), Molecular stratigraphy: A new tool for climatic assessment, *Nature*, *320*, 129–133.

Brown, S. J., and H. Elderfield (1996), Variations in Mg/Ca and Sr/Ca ratios of planktonic foraminifera caused by postdepositional dissolution: Evidence of shallow Mg-dependent dissolution, *Paleoceanography*, *11*, 543–551.

Bush, M. B., M. C. Miller, P. E. De Oliveira, and P. A. Colinvaux (2002), Orbital forcing signal in sediments of two Amazonian lakes, *J. Paleolimnol.*, *27*, 341–352.

Calvo, E., C. Pelejero, J. C. Herguera, A. Palanques, and J. O. Grimalt (2001a), Insolation dependence of the southeastern subtropical Pacific sea surface temperature over the last 400 kyrs, *Geophys. Res. Lett.*, *28*, 2481–2484.

Calvo, E., J. Villanueva, J. O. Grimalt, A. Boelaert, and L. Labeyrie (2001b), New insights into the glacial latitudinal temperature gradients in the North Atlantic. Results from $U^{K'}_{37}$ sea surface temperatures and terrigenous inputs, *Earth Planet. Sci. Lett.*, *188*, 509–519.

Carter, J. A., R. D. Garlick, P. Sutton, S. M. Chiswell, N. A. Oien, and B. R. Stanton (1998), *Ocean Circulation New Zealand*, *Misc. Chart Ser.*, vol. 76, Natl. Inst. of Water and Atmos. Res., Kilbirnie, Wellington, New Zealand.

Carter, L., and B. Manighetti (2006), Glacial/interglacial control of terrigenous and biogenic fluxes in the deep ocean off a high input, collisional margin: A 139 kyr-record from New Zealand, *Mar. Geol.*, *226*, 307–322.

Carter, L., B. Manighetti, M. Elliot, N. Trustrum, and B. Gomez (2002), Source, sea level and circulation effects on the sediment flux to the deep ocean over the past 15 ka off eastern New Zealand, *Global Planet. Change*, *33*, 339–355.

Cessi, P. (2000), Thermal feedback on wind stress as a contributing cause of climate variability, *J. Clim.*, *13*, 232–244.

Chapman, M. R., N. J. Shackleton, M. Zhao, and G. Eglinton (1996), Faunal and alkenone reconstructions of subtropical North Atlantic surface hydrography and paleotemperature over the last 28 kyr, *Paleoceanography*, *11*, 343–357.

Charles, C. D., D. Rind, J. Jouzel, R. D. Koster, and R. G. Fairbanks (1994), Glacial-interglacial changes in moisture sources for Greenland—Influences on the ice core record of climate, *Science*, *263*, 508–511.

Charles, C. D., J. Lynch-Stieglitz, U. S. Ninnemann, and R. G. Fairbanks (1996), Climate connections between the hemispheres revealed by deep sea sediment core/ice core correlations, *Earth Planet. Sci. Lett.*, *142*, 19–27.

Chiswell, S. M. (1996), Variability in the Southland Current, New Zealand, *N. Z. J. Mar. Freshwater Res.*, *30*, 1–17.

Chiswell, S. M. (2002), Temperature and salinity mean and variability within the Subtropical Front over the Chatham Rise, New Zealand, *N. Z. J. Mar. Freshwater Res.*, *36*, 281–298.

Conte, M. H., A. Thompson, D. Lesley, and R. P. Harris (1998), Genetic and physiological influences on the alkenone/alkenoate versus growth temperature relationship in *Emiliania huxleyi* and *Gephyrocapsa oceanica*, *Geochim. Cosmochim. Acta*, *62*, 51–68.

Cortese, G., and A. Abelmann (2002), Radiolarian-based paleotemperatures during the last 160 kyr at ODP Site 1089 (Southern Ocean, Atlantic Sector), *Palaeogeogr. Palaeoclimatol. Palaeoecol.*, *182*, 259–286.

Cortese, G., A. Abelmann, and R. Gersonde (2004), A glacial warm water anomaly in the subantarctic Atlantic Ocean, near the Agulhas Retroflection, *Earth Planet. Sci. Lett.*, *222*, 767–778.

Cortijo, E., S. Lehman, L. Keigwin, M. Chapman, D. Paillard, and L. Labeyrie (1999), Changes in meridional temperature and salinity gradients in the North Atlantic Ocean (30°N–72°N) during the last interglacial period, *Paleoceanography*, *14*, 23–33.

Cruz, F. W., S. J. Burns, I. Karmann, W. D. Sharp, M. Vuille, A. O. Cardoso, J. A. Ferrari, P. L. S. Dias, and O. Viana (2005), Insolation-driven changes in atmospheric circulation over the past 116,000 years in subtropical Brazil, *Nature*, *434*, 63–66.

Dannenmann, S., B. K. Linsley, D. W. Oppo, Y. Rosenthal, and L. Beaufort (2003), East Asian monsoon forcing of suborbital variability in the Sulu Sea during Marine Isotope Stage 3: Link to Northern Hemisphere climate, *Geochem. Geophys. Geosyst.*, *4*(1), 1001, doi:10.1029/2002GC000390.

Delaygue, G., V. Masson, J. Jouzel, R. D. Koster, and R. J. Healy (2000), The origin of Antarctic precipitation: A modelling approach, *Tellus, Ser. B*, *52*, 19–36.

Elderfield, H., and G. Ganssen (2000), Past temperature and $\delta^{18}O$ of surface ocean waters inferred from foraminiferal Mg/Ca ratios, *Nature*, *405*, 442–445.

Emeis, K.-C., D. M. Anderson, H. Doose, D. Kroon, and D. Schulz-Bull (1995), Sea-surface temperatures and the history of monsoon upwelling in the northwest Arabian Sea during the last 500,000 years, *Quat. Res.*, *43*, 355–361.

EPICA Community Members, (2004), Eight glacial cycles from an Antarctic ice core, *Nature*, *429*, 623–628.

Epstein, B. L., S. D'Hondt, J. G. Quinn, J. Zhang, and P. E. Hargraves (1998), An effect of dissolved nutrient concentrations on alkenone-based temperature estimates, *Paleoceanography*, *13*, 122–126.

Gallimore, R. G., and J. E. Kutzbach (1996), Role of orbitally induced changes in tundra area in the onset of glaciation, *Nature*, *381*, 503–505.

Gildor, H., and E. Tziperman (2000), Sea ice as the glacial cycles' climate switch: Role of seasonal and orbital forcing, *Paleoceanography*, *15*, 605–615.

Gildor, H., and E. Tziperman (2001), A sea ice climate switch mechanism for the 100-kyr glacial cycle, *J. Geophys. Res.*, *106*, 9117–9133.

Grootes, P. M., and M. Stuiver (1997), Oxygen 18/16 variability in Greenland snow and ice with 10^{-3}- to 10^{5}-year time resolution, *J. Geophys. Res.*, *102*, 26,455–26,470.

Gupta, S. M., A. A. Fernandes, and R. Mohan (1996), Tropical sea surface temperatures and the Earth's orbital eccentricity cycles, *Geophys. Res. Lett.*, *23*, 3159–3162.

Hallberg, R., and A. K. Inamdar (1992), Observations of seasonal variations in atmospheric greenhouse trapping and its enhancement at high sea surface temperature, *J. Clim.*, *6*, 920–931.

Heath, R. A. (1985), A review of the physical oceanography of the seas around New Zealand—1982, *N. Z. J. Mar. Freshwater Res.*, *19*, 79–124.

Herbert, T. D. (2003), Alkenone paleotemperature determinations, in *Treatise on Geochemistry*: vol. 6, *The Oceans and Marine Geochemistry*, edited by H. Elderfield, pp. 391–432, Elsevier, New York.

Herbert, T. D., J. D. Schuffert, D. Andreasen, L. Heusser, M. Lyle, A. C. Mix, A. C. Ravelo, L. D. Stott, and J. C. Herguera (2001), Collapse of the California Current during glacial maxima linked to climate change on land, *Science*, *293*, 71–76.

Herguera, J. C., and W. H. Berger (1991), Paleoproductivity from benthic foraminifera abundance: Glacial to postglacial change in the west-equatorial Pacific, *Geology*, *19*, 1173–1176.

Hodell, D. A., C. D. Charles, J. H. Curtis, P. G. Mortyn, U. S. Ninnemann, and K. A. Venz (2003), *Data Report: Oxygen Isotope Stratigraphy of ODP Leg 177 Sites 1088, 1089, 1090, 1093, and 1094*, edited by R. Gersonde,

D. A. Hodell, and P. Blum, Ocean Drill. Program, College Station, Tex. (Available at http://www-odp.tamu.edu/publications/177_SR/chap_09/chap_09.htm).

Howard, W. R., and W. L. Prell (1992), Late Quaternary surface circulation of the southern Indian Ocean and its relationship to orbital variations, *Paleoceanography*, *7*, 79–117.

Huybers, P., and C. Wunsch (2005), Obliquity pacing of the late Pleistocene glacial terminations, *Nature*, *434*, 491–494.

Ikehara, M., K. Kawamura, N. Ohkouchi, K. Kimoto, M. Murayama, T. Nakamura, T. Oba, and A. Taira (1997), Alkenone sea surface temperature in the Southern Ocean for the last two deglaciations, *Geophys. Res. Lett.*, *24*, 679–682.

Imbrie, J., et al. (1993), On the structure and origin of major glaciation cycles: 2. The 100,000-year cycle, *Paleoceanography*, *8*, 698–735.

Ishiwatari, R., M. Houtatsu, and H. Okada (2001), Alkenone-sea surface temperatures in the Japan Sea over the past 36 kyrs: Warm temperatures at the last glacial maximum, *Org. Geochem.*, *32*, 57–67.

Jasper, J., J. M. Hayes, A. C. Mix, and F. G. Prahl (1994), Photosynthetic fractionation of ^{13}C and concentrations of dissolved CO_2 in the central equatorial Pacific during the last 255,000 years, *Paleoceanography*, *9*, 781–798.

Johnson, R. G. (1991), Major Northern Hemisphere deglaciation caused by a moisture deficit 140 ka, *Geology*, *19*, 686–689.

Khodri, M., Y. Leclainche, G. Ramstein, P. Braconnot, O. Marti, and E. Cortijo (2001), Simulating the amplification of orbital forcing by ocean feedbacks in the last glaciation, *Nature*, *410*, 570–574.

King, A. L., and W. R. Howard (2001), Seasonality of foraminiferal flux in sediment traps at Chatham Rise, SW Pacific: Implications for paleotemperature estimates, *Deep Sea Res., Part I*, *48*, 1687–1708.

Kirst, G., R. Schneider, P. J. Müller, I. Von Storch, and G. Wefer (1999), Late Quaternary temperature variability in the Benguela Current system derived from alkenones, *Quat. Res.*, *52*, 92–103.

Laskar, J. (1990), The chaotic motion of the solar system: A numerical estimate of the size of the chaotic zones, *Icarus*, *88*, 226–291.

Lea, D. W., D. K. Pak, and H. J. Spero (2000), Climate impact of late Quaternary equatorial Pacific sea surface temperature variations, *Science*, *289*, 1719–1724.

Levitus, S., and T. Boyer (1994), *World Ocean Atlas 1994,* vol. 4, *Temperature*, *NOAA Atlas NESDIS 4*, 129 pp., Natl. Oceanic and Atmos. Admin., Silver Spring, Md.

Lewis, K. B., P. M. Barnes, J.-Y. Collot, B. Marcier de Lapinay, J. Delteil, and GeodyNZ Team (1999), *Central Hikurangi GeodyNZ Swath Maps*, *Misc. Chart Ser.*, vol. 77, Natl. Inst. of Water and Atmos. Res., Kilbirnie, Wellington, New Zealand.

Liu, Z., and T. D. Herbert (2004), High-latitude influence on the eastern equatorial Pacific climate in the early Pleistocene epoch, *Nature*, *427*, 720–723.

Loutre, M. F., D. Paillard, F. Vimeux, and E. Cortijo (2004), Does mean annual insolation have the potential to change the climate?, *Earth Planet. Sci. Lett.*, *221*, 1–14.

Madureira, L. A. S., S. A. van Kreveld, G. Eglinton, M. Conte, G. Ganssen, J. E. van Hinte, and J. J. Ottens (1997), Late Quaternary high-resolution biomarker and other sedimentary climate proxies in a northeast Atlantic core, *Paleoceanography*, *12*, 255–269.

Marlowe, I. T., J. C. Green, A. C. Neal, S. C. Brassell, G. Eglinton, and P. A. Course (1984), Long chain (n-C_{37}-C_{39}) alkenones in the prymnesiophyceae: Distribution of alkenones and other lipids and their taxonomic significance, *Br. Phycol. J.*, *19*, 203–216.

Mashiotta, T. A., D. W. Lea, and H. J. Spero (1999), Glacial-interglacial changes in subantarctic sea surface temperature and $\delta^{18}O$water using foraminiferal Mg, *Earth Planet. Sci. Lett.*, *170*, 417–432.

Masson-Delmotte, V., J. Jouzel, A. Landais, M. Stievenard, S. J. Johnsen, J. W. C. White, M. Werner, A. Sveinbjornsdottir, and K. Fuhrer (2005), GRIP deuterium excess reveals rapid and orbital-scale changes in Greenland moisture origin, *Science*, *309*, 118–121.

Mollenhauer, G., T. I. Eglinton, N. Ohkuchi, R. R. Schneider, P. J. Muller, P. M. Grootes, and J. Rullkotter (2003), Asynchronous alkenone and foraminifera records from the Benguela Upwelling System, *Geochim. Cosmochim. Acta*, *67*, 2157–2171.

Morley, J. J. (1989), Variations in high-latitude oceanographic fronts in the Southern Indian Ocean: An estimation based on faunal changes, *Paleoceanography*, *4*, 547–554.

Müller, P. J., M. Cepek, G. Ruhland, and R. R. Schneider (1997), Alkenone and coccolithophorid species changes in late Quaternary sediments from the Walvis Ridge: Implications for the alkenone paleotemperature method, *Palaeogeogr. Palaeoclimatol. Palaeoecol.*, *135*, 71–96.

Müller, P. J., G. Kirst, G. Ruhland, I. von Storch, and A. Rosell-Mele (1998), Calibration of the alkenone paleotemperature index $U^{k'}_{37}$ based on core-tops from the eastern South Atlantic and the global ocean (60°N–60°S), *Geochim. Cosmochim. Acta*, *62*, 1757–1772.

Nelson, C. S., I. L. Hendy, H. L. Neil, C. H. Hendy, and P. P. E. Weaver (2000), Last glacial jetting of cold waters through the Subtropical Convergence zone in the southwest Pacific off eastern New Zealand, and some geological implications, *Palaeogeogr. Palaeoclimatol. Palaeoecol.*, *156*, 103–121.

Ninnemann, U. S., and C. D. Charles (2002), Change in the mode of Southern Ocean circulation over the last glacial cycle revealed by foraminiferal stable isotopic variability, *Earth Planet. Sci. Lett.*, *201*, 383–396.

Ninnemann, U. S., C. D. Charles, and D. A. Hodell (1999), Origin of global millennial scale climate events: Constraints from the Southern Ocean deep sea sedimentary record, in *Mechanisms of Global Climate Change at Millennial Time Scales*, *Geophys. Monogr. Ser.*, vol. 112, edited by P. U. Clark, R. S. Webb, and L. D. Keigwin, pp. 99–112, AGU, Washington, D. C.

NorthGRIP Members, (2004), High-resolution record of Northern Hemisphere climate extending into the last interglacial period, *Nature*, *431*, 147–151.

Nürnberg, D. (1995), Magnesium in tests of *Neogloboquadrina pachyderma* sinistral from high northern and southern latitudes, *J. Foraminiferal Res.*, *25*, 350–368.

Nürnberg, D., J. Bijma, and C. Hemleben (1996), Assessing the reliability of magnesium in foraminiferal calcite as a proxy for water mass temperatures, *Geochim. Cosmochim. Acta*, *60*, 803–814.

Nürnberg, D., A. Müller, and R. R. Schneider (2000), Paleo-sea surface temperature calculations in the Equatorial East Atlantic from Mg/Ca ratios in planktic foraminifera: A comparison to sea surface temperature estimates from $U^{K'}_{37}$, oxygen isotopes, and foraminiferal transfer function, *Paleoceanography*, *15*, 124–134.

Ohkouchi, N., K. Kawamura, H. Kawahata, and H. Okada (1999), Depth ranges of alkenone production in the central Pacific Ocean, *Global Biogeochem. Cycles*, *13*, 695–704.

Ohkouchi, N., T. I. Eglinton, L. D. Keigwin, and J. M. Hayes (2002), Spatial and temporal offsets between proxy records in a sediment drift, *Science*, *298*, 1224–1227.

Pahnke, K., and R. Zahn (2005), Southern Hemisphere water mass conversion linked with North Atlantic climate variability, *Science*, *307*, 1741–1746.

Pahnke, K., R. Zahn, H. Elderfield, and M. Schulz (2003), 340,000-year centennial-scale marine record of Southern Hemisphere climatic oscillation, *Science*, *301*, 948–952.

Pailler, D., and E. Bard (2002), High frequency palaeoceanographic changes during the past 140,000 yr recorded by the organic matter in sediments of the Iberian Margin, *Palaeogeogr. Palaeoclimatol. Palaeoecol.*, *181*, 431–452.

Peixoto, J. P., and A. H. Oort (1992), *Physics of Climate*, 520 pp., Am. Inst. Phys., New York.

Pelejero, C., J. O. Grimalt, S. Heilig, M. Kienast, and L. J. Wang (1999), High-resolution $U^{K'}_{37}$ temperature reconstructions in the South China Sea over the past 220 kyr, *Paleoceanography*, *14*, 224–231.

Perks, H. M., C. D. Charles, and R. F. Keeling (2002), Precessionally forced productivity variations across the equatorial Pacific, *Paleoceanography*, *17*(3), 1037, doi:10.1029/2000PA000603.

Petit, J. R., et al. (1999), Climate and atmospheric history of the past 420,000 years from the Vostok ice core, Antarctica, *Nature*, *399*, 429–436.

Pichevin, L., M. Cremer, J. Giraudeau, and P. Bertrand (2005), A 190 ky record of lithogenic grain-size on the Namibian slope: Forging a tight link between past wind-strength and coastal upwelling dynamics, *Mar. Geol.*, *218*, 81–96.

Pichon, J. J., E. L. Sikes, C. Hiramatsu, and L. Robertson (1998), Comparison of $U^{K'}_{37}$ and diatom assemblage sea surface temperature estimates with atlas derived data in Holocene sediments from the Southern West Indian Ocean, *J. Mar. Syst.*, *17*, 541–554.

Pierrehumbert, R. T. (1999), Subtropical water vapor as a mediator of rapid global climate change, in *Mechanisms of Global Climate Change at Millennial Time Scales*, *Geophys. Monogr. Ser.*, vol. 112, edited by P. U. Clark, R. S. Webb, and L. Keigwin, pp. 339–360, AGU, Washington, D. C.

Prahl, F. G., and S. G. Wakeham (1987), Calibration of unsaturation patterns in long-chain ketone compositions for paleotemperature assessment, *Nature*, *330*, 367–369.

Prahl, F. G., L. A. Muehlhausen, and D. L. Zahnle (1988), Further evaluation of long-chain alkenones as indicators of paleoceanographic conditions, *Geochim. Cosmochim. Acta*, *52*, 2303–2310.

Prahl, F. G., R. B. Collier, J. Dymond, M. Lyle, and M. A. Sparrow (1993), A biomarker perspective on prymnesiophyte productivity in the northeast Pacific Ocean, *Deep Sea Res., Part I*, *40*, 2061–2076.

Prahl, F. G., B. N. Popp, D. M. Karl, and M. A. Sparrow (2005), Ecology and biogeochemistry of alkenone production at Station ALOHA, *Deep Sea Res., Part I*, *52*, 699–719.

Raymo, M. E., and K. Nisancioglu (2003), The 41 kyr world: Milankovitch's other unsolved mystery, *Paleoceanography*, *18*(1), 1011, doi:10.1029/2002PA000791.

Reijmer, C. H., M. R. van den Broeke, and M. P. Scheele (2002), Air parcel trajectories and snowfall related to five deep drilling locations in Antarctica based on the ERA-15 dataset, *J. Clim.*, *15*, 1957–1968.

Roemmich, D., and P. Sutton (1998), The mean and variability of ocean circulation past northern New Zealand: Determining the representativeness of hydrographic climatologies, *J. Geophys. Res.*, *103*, 13,041–13,054.

Rostek, F., G. Ruhland, F. C. Bassinot, P. J. Muller, L. D. Labeyrie, Y. Lancelot, and E. Bard (1993), Reconstructing sea-surface temperature and salinity using delta-O-18 and alkenone records, *Nature*, *364*, 319–321.

Rostek, F., E. Bard, L. Beaufort, C. Sonzogni, and G. Ganssen (1997), Sea surface temperature and productivity records for the past 240 kyr in the Arabian Sea, *Deep Sea Res., Part II*, *44*, 1461–1480.

Sachs, J. P., and R. F. Anderson (2003), Fidelity of alkenone paleotemperatures in southern Cape Basin sediment drifts, *Paleoceanography*, *18*(4), 1082, doi:10.1029/2002PA000862.

Sachs, J. P., and R. F. Anderson (2005), Increased productivity in the subantarctic ocean during Heinrich events, *Nature*, *434*, 1118–1121.

Sachs, J. P., and S. J. Lehman (1999), Subtropical North Atlantic temperatures 60,000 to 30,000 years ago, *Science*, *286*, 756–759.

Sachs, J. P., R. R. Schneider, T. I. Eglinton, K. H. Freeman, G. Ganssen, J. F. McManus, and D. W. Oppo (2000), Alkenones as paleoceanographic proxies, *Geochem. Geophys. Geosyst.*, *1*, doi:10.1029/2000GC000059.

Sachs, J. P., R. F. Anderson, and S. J. Lehman (2001), Glacial surface temperatures of the southeast Atlantic ocean, *Science*, *293*, 2077–2079.

Schmidt, M. W., H. J. Spero, and D. W. Lea (2004), Links between salinity variation in the Caribbean and North Atlantic thermohaline circulation, *Nature*, *428*, 160–163.

Schneider, R. R., P. J. Müller, and G. Ruhland (1995), Late Quaternary surface circulation in the east-equatorial South Atlantic: Evidence from alkenone sea surface temperatures, *Paleoceanography*, *10*, 197–219.

Schneider, R. R., P. J. Müller, and R. Acheson (1999), Atlantic alkenone sea-surface temperature records: Low versus mid latitudes and differences between hemispheres, in *Reconstructing Ocean History: A Window Into the Future*, edited by F. Abrantes and A. C. Mix, pp. 33–55, Springer, New York.

Schrag, D. P., J. F. Adkins, K. McIntyre, J. L. Alexander, D. A. Hodell, C. D. Charles, and J. F. McManus (2002), The oxygen isotopic composition of seawater during the Last Glacial Maximum, *Quat. Sci. Rev.*, *21*, 331–342.

Schulte, S., and P. J. Müller (2001), Variations in sea-surface temperature and primary productivity during Heinrich and Dansgaard-Oeschger events in the northeastern Arabian Sea, *Geo Mar. Lett.*, *21*, 168–175.

Schulte, S., F. Rostek, E. Bard, J. Rullkoetter, and O. Marchal (1999), Variations of oxygen-minimum and primary productivity recorded in sediments of the Arabian Sea, *Earth Planet. Sci. Lett.*, *173*, 205–221.

Seki, O., K. Kawamura, M. Ikehara, T. Nakatsuka, and T. Oba (2004), Variation of alkenone sea surface temperature in the Sea of Okhotsk over the last 85 kyrs, *Org. Geochem.*, *35*, 347–354.

Shackleton, N. J. (2000), The 100,000-year ice-age cycle identified and found to lag temperature, carbon dioxide, and orbital eccentricity, *Science*, *289*, 1897–1902.

Shackleton, N. J., M. A. Hall, and E. Vincent (2000), Phase relationships between millennial-scale events 64,000–24,000 years ago, *Paleoceanography*, *15*, 565–569.

Shane, P., and A. Sandiford (2003), Paleovegetation of marine isotope stages 4 and 3 in Northern New Zealand and the age of the widespread Rotoehu tephra, *Quat. Res.*, *59*, 420–429.

Sicre, M. A., Y. Ternois, M. Paterne, A. Boireau, L. Beaufort, P. Martinez, and P. Bertrand (2000), Biomarker stratigraphic records over the last 150 kyrs off the NW African coast at 25°N, *Org. Geochem.*, *31*, 577–588.

Sikes, E. L., and L. D. Keigwin (1994), Equatorial Atlantic sea surface temperatures for the last 30 ky: A comparison of $U^{K'}_{37}$, $\delta^{18}O$, and foraminiferal assemblage estimates, *Paleoceanography*, *9*, 31–46.

Sikes, E. L., and L. D. Keigwin (1996), A reexamination of northeast Atlantic sea surface temperature and salinity over the last 16 kyr, *Paleoceanography*, *11*, 327–342.

Sikes, E. L., and J. K. Volkman (1993), Calibration of alkenone unsaturation ratios ($U^{K'}_{37}$) for paleotemperature estimation in cold polar waters, *Geochim. Cosmochim. Acta*, *57*, 1883–1889.

Sikes, E. L., J. K. Volkman, L. G. Robertson, and J.-J. Pichon (1997), Alkenones and alkenes in surface waters and sediments of the Southern Ocean: Implications for paleotemperature estimation in polar regions, *Geochim. Cosmochim. Acta*, *61*, 1495–1505.

Sikes, E. L., W. R. Howard, H. L. Neil, and J. K. Volkman (2002), Glacial-interglacial sea surface temperature changes across the subtropical front east of New Zealand based on alkenone unsaturation ratios and foraminiferal assemblages, *Paleoceanography*, *17*(2), 1012, doi:10.1029/2001PA000640.

Sikes, E. L., T. O'Leary, S. D. Nodder, and J. K. Volkman (2005), Alkenone temperature records and biomarker flux at the subtropical front on the Chatham Rise, SW Pacific Ocean, *Deep Sea Res., Part I*, *52*, 721–748.

Stoner, J. S., J. E. T. Channell, D. A. Hodell, and C. D. Charles (2003), A ~580 kyr paleomagnetic record from the sub-Antarctic South Atlantic (Ocean Drilling Program Site 1089), *J. Geophys. Res.*, *108*(B5), 2244, doi:10.1029/2001JB001390.

Sutton, P. (2001), Detailed structure of the Subtropical Front over Chatham Rise, east of New Zealand, *J. Geophys. Res.*, *106*, 31,045–31,056.

Ternois, Y., M.-A. Sicre, A. Boireau, L. Beaufort, J.-C. Miquel, and C. Jeandel (1998), Hydrocarbons, sterols and alkenones in sinking particles in the Indian Ocean sector of the Southern Ocean, *Org. Geochem.*, *28*, 489–501.

Thunell, R. C., and S. Honjo (1981), Calcite dissolution and the modification of planktonic foraminiferal assemblages, *Mar. Micropaleontol.*, *6*, 169–182.

Tucholke, B. E., and R. W. Embley (Eds.) (1984), Cenozoic regional erosion of the abyssal sea floor off South Africa, in *Interregional Unconformities and Hydrocarbon Accumulation*, *Memoirs*, vol. 36, 145–164 pp., Am. Assoc. of Petrol. Geol., Tulsa, Okla.

Uddstrom, M. J., and N. A. Oien (1999), On the use of high-resolution satellite data to describe the spatial and temporal variability of sea surface temperatures in the New Zealand region, *J. Geophys. Res.*, *104*, 20,729–20,751.

van Campo, E., J. C. Duplessy, W. L. Prell, N. Barratt, and R. Sabatier (1990), Comparison of terrestrial and marine temperature estimates for the past 135 kyr off southeast Africa: A test for GCM simulations of paleoclimate, *Nature*, *348*, 209–212.

Villanueva, J., J. O. Grimalt, E. Cortijo, L. Vidal, and L. Labeyrie (1998), Assessment of sea surface temperature variations in the central North Atlantic using the alkenone unsaturation index ($U^{K'}_{37}$), *Geochim. Cosmochim. Acta*, *62*, 2421–2427.

Villanueva, J., J. A. Flores, and J. O. Grimalt (2002), A detailed comparison of the $U^{K'}_{37}$ and coccolith records over the past 290 years: Implications to the alkenone paleotemperature method, *Org. Geochem.*, *33*, 897–905.

Vimeux, F., V. Masson, J. Jouzel, M. Stievenard, and J. R. Petit (1999), Glacial-interglacial changes in ocean surface conditions in the Southern Hemisphere, *Nature*, *398*, 410–413.

Vimeux, F., V. Masson, G. Delaygue, J. Jouzel, J. R. Petit, and M. Stievenard (2001), A 420,000 year deuterium excess record from East Antarctica: Information on past changes in the origin of precipitation at Vostok, *J. Geophys. Res.*, *106*, 31,863–31,873.

Vimeux, F., K. M. Cuffey, and J. Jouzel (2002), New insights into Southern Hemisphere temperature changes from Vostok ice cores using deuterium excess correction, *Earth Planet. Sci. Lett.*, *203*, 829–843.

Volkman, J. K., G. Eglinton, E. D. S. Corner, and T. E. V. Forsberg (1980), Long-chain alkenes and alkenones in the marine coccolithophorid *Emiliania huxleyi*, *Phytochemistry*, *19*, 2619–2622.

Volkman, J. K., S. M. Barrett, S. I. Blackburn, and E. L. Sikes (1995), Alkenones in *Gephyrocapsa oceanica*: Implications for studies of paleoclimate, *Geochim. Cosmochim. Acta*, *59*, 513–520.

Watkins, J. M., and A. C. Mix (1998), Testing the effects of tropical temperature, productivity, and mixed-layer depth on foraminiferal transfer functions, *Paleoceanography*, *13*, 96–105.

Weaver, P. P. E., L. Carter, and H. L. Neil (1998), Response of surface water masses and circulation to late Quaternary climate change east of New Zealand, *Paleoceanography*, *13*, 70–83.

Weaver, P. P. E., M. Chapman, G. Eglinton, M. Zhao, D. Rutledge, and G. Read (1999), Combined coccolith, foraminiferal, and biomarker reconstruction of paleoceanographic conditions over the past 120 kyr in the northern North Atlantic (59°N, 23°W), *Paleoceanography*, *14*, 336–349.

Wells, P., and H. Okada (1997), Response of nanoplankton to major changes in sea-surface temperature and movements of hydrological fronts over Site DSDP 594 (South Chatham Rise, southeastern New Zealand), during the last 130 kyr, *Mar. Micropaleontol.*, *32*, 341–363.

Wells, P. E., and G. M. Wells (1994), Large-scale reorganization of ocean currents offshore Western Australia during the Late Quaternary, *Mar. Micropaleontol.*, *24*, 157–186.

Wolff, T., B. Grieger, W. Hale, A. Dürkoop, S. Mulitza, J. Pätzold, and G. Wefer (1999), On the reconstruction of paleosalinities, in *Use of Proxies in Paleoceanography: Examples from the South Atlantic*, edited by G. Fischer and G. Wefer, pp. 207–228, Springer, New York.

Yamamoto, M., T. Oba, J. Shimamune, and T. Ueshima (2004), Orbital-scale anti-phase variation of sea surface temperature in mid-latitude North Pacific margins during the last 145,000 years, *Geophys. Res. Lett.*, *31*, L16311, doi:10.1029/2004GL020138.

Zhao, M., N. A. S. Beveridge, N. J. Shackleton, M. Sarnthein, and G. Eglinton (1995), Molecular stratigraphy of cores off northwest Africa: Sea surface temperature history over the last 80 ka, *Paleoceanography*, *10*, 661–675.

Zielinski, U., R. Gersonde, R. Sieger, and D. K. Fütterer (1998), Quaternary surface water temperature estimations: Calibration of a diatom transfer function for the Southern Ocean, *Paleoceanography*, *13*, 365–383.

K. Pahnke, Lamont-Doherty Earth Observatory of Columbia University, Palisades, NY 10964, USA. (kpahnke@ldeo.columbia.edu)

J. Sachs, School of Oceanography, University of Washington, Seattle, WA 98195, USA. (jsachs@u.washington.edu)